



# **JGR Space Physics**



#### RESEARCH ARTICLE

10.1029/2022JA030375

#### **Key Points:**

- Properties of dark band structures representing nighttime medium-scale traveling ionospheric disturbances (MSTIDs) observed over South Africa presented for the first time
- MSTIDs prevalent in southern hemisphere winter and primarily propagated westward
- Occurrence of MSTIDs is mostly accompanied by sporadic and spread-F, while propagation is supported by favorable neutral wind circulation

#### Correspondence to:

Z. T. Katamzi-Joseph, zkatamzi@sansa.org.za

#### Citation:

Katamzi-Joseph, Z. T., Grawe, M. A., Makela, J. J., Habarulema, J. B., Martinis, C., & Baumgardner, J. (2022). First results on characteristics of nighttime MSTIDs observed over South Africa: Influence of thermospheric wind and sporadic E. *Journal of Geophysical Research: Space Physics*, 127, e2022JA030375. https://doi.org/10.1029/2022JA030375

Received 10 FEB 2022 Accepted 7 OCT 2022

© 2022. The Authors.

This is an open access article under the terms of the Creative Commons Attribution-NonCommercial-NoDerivs License, which permits use and distribution in any medium, provided the original work is properly cited, the use is non-commercial and no modifications or adaptations are made.

# First Results on Characteristics of Nighttime MSTIDs Observed Over South Africa: Influence of Thermospheric Wind and Sporadic E

Z. T. Katamzi-Joseph<sup>1,2</sup>, M. A. Grawe<sup>3,4</sup>, J. J. Makela<sup>3</sup>, J. B. Habarulema<sup>1,2</sup>, C. Martinis<sup>5</sup>, and J. Baumgardner<sup>5</sup>

<sup>1</sup>South African National Space Agency (SANSA), Hermanus, South Africa, <sup>2</sup>Department of Physics & Electronics, Rhodes University, Makhanda, South Africa, <sup>3</sup>Department of Electrical and Computer Engineering, University of Illinois at Urbana-Champaign, Urbana, IL, USA, <sup>4</sup>Now at Applied Physics Laboratory, Johns Hopkins University, Laurel, MD, USA, <sup>5</sup>Center for Space Physics, Boston University, Boston, MA, USA

**Abstract** This paper reports the climatology of medium-scale traveling ionospheric disturbances (MSTIDs) observed between September 2018 and August 2019 in the nighttime redline airglow intensity measurements from an all-sky imager located in Sutherland, South Africa (32.4°S, 20.8°E; magnetic latitude: 40.7°S). The nighttime MSTIDs appeared as either single or multiple dark bands, commenced mostly before midnight, and predominantly occurred during the southern winter solstice. They primarily propagated westward with speeds of 31–127 m/s. The periods and wavelengths of the multi-band MSTIDs were in the ranges of 26–155 min and 134–578 km, respectively, while the temporal and spatial scales of the single band MSTIDs were 11–30 min and 43–143 km, respectively. Analysis of neutral wind measurements from a co-located Fabry-Perot interferometer showed that the thermospheric wind was mostly northeastward in the evenings of MSTID occurrence and that the favored westward propagation of the MSTIDs was the least restricted propagation direction by the background wind. Based on data from nearby ionosondes, the MSTIDs were mostly accompanied by sporadic E and spread-F structures. From the seasonal occurrences of MSTIDs and sporadic E as well as the MSTID propagation and prevalent wind directions, it is concluded that Perkins instability is the most likely source of the majority of the observed nighttime MSTIDs, while the remainder may be seeded by gravity waves.

#### 1. Introduction

Medium-scale traveling ionospheric disturbances (MSTIDs) are propagating electron density oscillations found in the ionospheric F region. Their occurrence is typically ascribed to atmospheric gravity waves (AGWs) or electromagnetic instabilities. These wave-like perturbations have been extensively investigated using a wide range of methods such as backscatter echoes from HF radars like SuperDARN (e.g., Bristow et al., 1996; He et al., 2004; Oinats et al., 2015), airglow imaging of 630.0 nm by all-sky imagers (e.g., Garcia et al., 2000; Makela et al., 2010; Martinis et al., 2019; Otsuka et al., 2004; Rajesh et al., 2016; Shiokawa et al., 2003), and total electron content from global navigation satellite systems or low-earth satellites such as Swarm (e.g., Ding et al., 2011; Kil & Paxton, 2017; Kotake et al., 2006; Otsuka et al., 2013) as well as a combination of such instruments (e.g., Huang et al., 2016, 2018). Prior studies of these disturbances revealed typical characteristics in period, horizontal velocity and wavelength in the ranges of approximately 10-60 min, 50-300 m/s and 100-400 km, respectively (e.g., Hunsucker, 1982; Jacobson et al., 1995; Mayr et al., 1984). They have propagation directions that largely vary, which suggests that the mechanisms through which they are generated also differ. For example, Tsugawa, Otsuka, et al. (2007) presented MSTIDs over North America which propagated toward south-southeastward during the daytime and southwestward during the nighttime. They linked the daytime MSTIDs to wind filtering effect of AGWs and the nighttime MSTIDs to electrodynamical forces. A climatological study by Ding et al. (2011) found that daytime MSTIDs propagated mostly equatorward but the nighttime MSTIDs propagated southwestward over China. In Australia and over the South American sector Shiokawa et al. (2005) and Pimenta, Kelley, et al. (2008), respectively, observed northwest propagating nighttime MSTIDs. Also, Grocott et al. (2013) reported on equatorward traveling MSTIDs over the Antarctic Peninsula that they linked to enhanced solar wind-magnetosphere coupling. They also reported westward propagating TIDs which they suggested were excited by winds over mountain ranges or the Antarctic polar vortex. Clearly these and other studies show that the propagation direction

KATAMZI-JOSEPH ET AL. 1 of 20

of daytime MSTIDs may be varied, however MSTIDs that are observed at nighttime generally propagate equatorward and to the west in both hemispheres, that is, northwest (southwest) in the southern (northern) hemisphere (e.g., Jacobson et al., 1995; Makela et al., 2010; Martinis et al., 2019; Mendillo et al., 1997; Shiokawa et al., 2012; Tsugawa, Kotake, et al., 2007).

Studies also show that in addition to this preferred direction of propagation, nighttime MSTIDs have phase fronts aligned in the northeast-southwest (northwest-southeast) in the southern (northern) hemisphere. This preferred alignment led to the suggestion of the Perkins instability (Perkins, 1973) as the mechanism through which these disturbances are generated (e.g., Kelley, 2011; Kelley & Miller, 1997; Miller et al., 1997; Shiokawa et al., 2003). The Perkins instability predicts that the nighttime F region, which is supported by the  $\mathbf{E} \times \mathbf{B}$  force against gravity, becomes unstable if a north-south electric field component exists in addition to the equilibrium eastward field. The growth rate of this instability is mainly dependent on the angles of both the equilibrium electric field and perturbation wave vector to magnetic east and possibly the dip angle of the magnetic field, although the extent of the latter dependency is currently not well known. To improve the physical explanation and interpretation of the Perkins instability process, the theory was further developed to include the presence of the neutral wind (e.g., Hamza, 1999; Zhou & Matthews, 2006).

Further evidence of the role of the Perkins instability in the generation of nighttime MSTIDs, sometimes called electrified MSTIDs, was revealed by simultaneous observations of these structures at geomagnetic conjugate stations in both hemispheres. The pioneering work that illustrated this was presented by Otsuka et al. (2004) who reported conjugate MSTIDs in images made observing the 630.0 nm airglow layer from Japan and Australia. They concluded that electric fields, induced to maintain divergent-free electric current in the presence of MSTID-perturbed Pedersen conductivity, map along the magnetic field lines and cause plasma density perturbations in the opposite hemisphere via  $\mathbf{E} \times \mathbf{B}$  plasma drift. Subsequent work reporting more observations of conjugate MSTIDs again emphasized the important role played by electrodynamical forces in the creation of these structures (e.g., Burke et al., 2016; Kotake et al., 2006; Martinis et al., 2011, 2019; Narayanan et al., 2018; Shiokawa et al., 2005; Shiokawa et al., 2009).

There is, however, a concern on the efficiency of the Perkins instability in enabling the generation of the night-time MSTIDs due to its growth rate being too small/slow (e.g., Hamza, 1999; Kelley & Makela, 2001). Kelley and Fukao (1991) and Huang et al. (1994) suggested, as one possibility, the seeding by AGWs to reinforce the slow growth rate by inducing electric fields in the E region or opposite hemisphere. These electric fields would then map to the F region along the magnetic field lines where they enhance the Perkins instability. The other suggested possibility is seeding by the coupled electrodynamics between E and F regions (e.g., Cosgrove & Tsunoda, 2002, 2004; Tsunoda & Cosgrove, 2001; Yokoyama et al., 2009). The coupled E-F instability mechanism involves sporadic E initiating a Hall current driven polarization process with the polarization electric fields mapped to the F-region along the magnetic field lines. The Hall driven electric fields enhance the polarization electric fields generated by the Perkins instability resulting in the strengthening of the MSTIDs that initiated the sporadic E. This process allows the instabilities to grow faster since they are reinforced by this mutual positive feedback. The viability of this process is supported by the fact that sporadic E shows a similar directional alignment as the MSTIDs wave fronts, is often observed simultaneously with the MSTIDs and has similar periodicity and propagation direction (e.g., Kelley et al., 2003; Narayanan et al., 2018; Otsuka et al., 2007; Saito et al., 2007; Yamamoto et al., 1994; Yokoyama et al., 2004).

Many of the existing climatological studies of nighttime MSTIDs have been conducted in the American, Asian-Pacific and European sectors, with no such studies covering the African sector primarily due to lack of suitable instrumentation. Although there are similarities in these climatologies, there are also differences and discrepancies. For example, whereas Kotake et al. (2007), Shiokawa et al. (2003), Ding et al. (2011), and Huang et al. (2016) found that the occurrence of the nighttime MSTIDs peaked during the June solstice over South-West USA, Japan and China, respectively, Garcia et al. (2000) observed peak occurrence during the December solstice over Puerto Rico, while Shiokawa et al. (2003), Martinis et al. (2010), Duly et al. (2013), and Otsuka et al. (2013) showed peaks in both the June and December solstices over Japan, Puerto Rico, Hawaii, and Europe, respectively, as did Kil and Paxton (2017) in a global distribution covering both hemispheres. Therefore, further studies of nighttime MSTIDs are essential to bridge the knowledge gap in their distribution and factors contributing to the mechanisms through which they are generated. This study presents the first climatology of nighttime MSTID

KATAMZI-JOSEPH ET AL. 2 of 20

21699402, 2022, 11, Downloaded from https://agupubs.onlinelibrary.wiley.com/doi/10.1029/2022IA030375 by Boston University, Wiley Online Library on [23/06/2023]. See

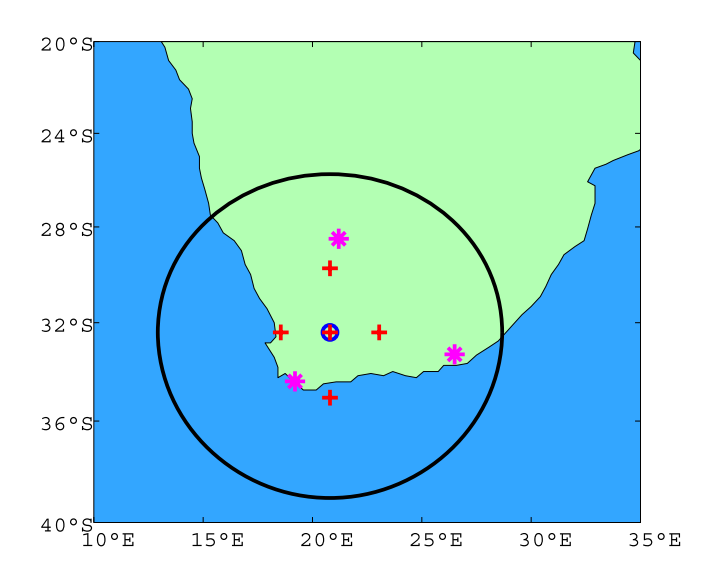


**Figure 1.** Location of the all-sky imager (ASI) (blue circle), Fabry-Perot interferometer and its look directions (red cross) as well as the ionosondes (magenta asterisk) in South Africa. Black circle indicates the field of view of the ASI for the 630.0 nm airglow emissions.

occurrence over South Africa during quiet geomagnetic conditions using data collected during the period of September 2018 to August 2019.

#### 2. Data and Method

In this study we used measurements of the airglow emission at a wavelength of 630.0 nm (OI redline) made by an all-sky imager (ASI) located at the South African Astronomical Observatory in Sutherland, South Africa (32.4°S, 20.8°E; magnetic latitude: 40.7°S). This imager, whose location is shown in Figure 1, is part of the Boston University's imaging network, described in detail in Martinis et al. (2018). Its field of view at a zenith angle of  $80^\circ$ , assuming an emission height of 250 km for OI airglow, is ~1,400 km and is shown by the black circle in Figure 1. The measurements used in this study were taken every 11 min with an exposure time of 120 s. Processed images were produced by subtracting the background emission, observed at a wavelength of 605 nm, and projecting the images to geographic coordinates based on spatial calibration made using stellar calibration (e.g., Mondal et al., 2019; Sangalli et al., 2011).

The Sutherland imager is co-located with a narrow field of view (~1.8°) Fabry-Perot interferometer (FPI) as shown in Figure 1. This instrument measures the temperature and motion of neutrals in the upper atmosphere from line of sight Doppler broadening and shift of the spectral line shape

of the 630.0 nm airglow emission. The measurements are collected in the standard cardinal mode, a cyclical process of taking measurements in the north, east, south, and west directions at a 45° elevation angle followed by observations in the zenith direction, and lastly by frequency-stabilized laser observations that are used for monitoring of the instrument function. The FPI instrument design and data processing is described in detail by Fisher et al. (2015). This study only used the neutral wind measurements to study its influence on propagation of MSTIDs, while Ojo et al. (2022) used data from the same instrument to present a general seasonal wind variation as well as validation of the horizontal wind model, version 2014 (HWM14).

In addition to the optical measurements, we used ionograms from ionosondes to obtain sporadic E and spread-F information and determine a connection of E-F region instabilities with occurrence of MSTIDs. While none of the ionosondes from the South African ionosonde network are co-located with the Sutherland optical instruments,

Table 1
Number of Nights When Observations Were Made, With Clear Night
Conditions and When Medium-Scale Traveling Ionospheric Disturbances
(MSTIDs) Were Observed Between September 2018 and August 2019

Month	Observations	Clear sky	MSTIDs
September	25	8	2
October	28	11	3
November	27	15	3
December	25	12	1
January	27	3	1
February	26	12	4
March	22	14	3
April	23	17	3
May	25	10	1
June	20	7	3
July	28	7	6
August	24	13	9

three of them are located within the field of view of the ASI instrument. These ionosondes are located in Grahamstown (GR13L: 33.3°S, 26.6°E), Hermanus (HE13N: 34.4°S, 19.2°E) and Louisvale (LV12P: 28.5°S, 21.2°E). Ionosonde measurements with a cadence of 15 min were obtained from the Global Ionospheric Radio Observatory database (Reinisch & Galkin, 2011).

In Sutherland, airglow images have been collected continuously since July 2016, while FPI wind observations commenced in January 2018. Therefore, in order to get an overlapping continuous 1 year of data from both instruments for this study, data between September 2018 and August 2019 were used. Since the ASI and FPI are optical instruments, their measurements are only reliable during clear sky conditions at night. The occurrence of these conditions in each month of this study period are summarized in Table 1 and Figure 2a, while Figure 2b shows the seasonal variation. The total number of nights of observations exclude nights with clear images for less than an hour and when geomagnetic conditions were disturbed, as defined by 3-hourly Kp > 4 and/or hourly Dst  $\leq -30$  nT. Clear sky conditions refer to images without cloud coverage or moonlight contamination for at least 60% of the nightly observation duration. Nights are also removed from consideration when the instrument malfunctioned resulting in bad, out of focus or blank images. Table 1 and Figure 2 indicate relatively good observation conditions over Sutherland with an average clear sky condition on 44% of nights. Most

KATAMZI-JOSEPH ET AL. 3 of 20

21699402, 2022, 11, Downloaded from https://agupubs.onlinelibrary.wiley.com/doi/10.1029/2021A030375 by Boston University, Wiley Online Library on [23/06/2023]. See the Terms

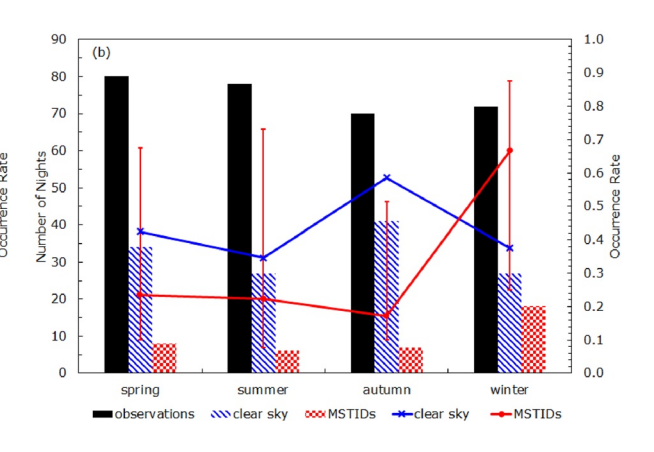


**Figure 2.** Number of nights when observations were made (black), sky conditions were clear (blue), medium-scale traveling ionospheric disturbances were observed (red) as well as their occurrence rates indicated on secondary/right *y*-axis and given by the blue and red curves. (a) Shows monthly statistics, while (b) shows seasonal statistics.

0.9

0.4

0.3

0.1

months had clear sky occurrence rate, indicated by the blue curve in Figure 2a, of at least 30%, except for January and July. Note the occurrence rate of clear sky is calculated as the ratio of clear sky nights to the observation nights and indicated by the secondary (right) y-axis of Figure 2. Seasons are divided as follows: spring (September–November), summer (December–February), autumn (March–May), and winter (June–August). The nights with clear skies are most likely to occur during autumn.

#### 3. Results

■observations SSS clear sky MSTIDs →-clear sky

Depending on the season, the optical observations were taken starting between  $\sim 1630-1910$  UT (1753–2033 LT, where LT is the solar local time calculated as LT = UT +  $24\frac{long tinude}{360}$ ) and ending between  $\sim 0220-0450$  UT (0346–0613 LT). Nighttime MSTIDs were identified through visual inspection of the processed images. As shown in Table 1, MSTIDs were observed on 39 nights out of a total of 129 clear sky nights, meaning that they were observed in roughly 30% of nights with clear-sky and quiet geomagnetic conditions. To ensure that the detected nighttime MSTIDs are indeed F-region structures, we checked for similar structures in the 557.7 and 695.0 nm images collected by the ASI on the same night. Structures that appeared in 630.0 nm and 557.7 or 695.0 nm were excluded from the study.

The nighttime MSTIDs observed in this study appeared as either single or multiple dark band structures in airglow images. A total of 43 MSTIDs were identified in 39 nights, meaning some nights had multiple MSTID events which were identified as such if the bands of these structures either propagated in different directions or were observed at different times on the same night and had very different characteristics, that is, speed and wavelength/spatial scale. The results shown in Table 1 and Figure 2 indicate that for most of the year, MSTIDs were observed on only a few nights in each month. The exception is during July and August when MSTIDs were observed with occurrence rates of \$\ge 70\%. This occurrence trend means that the MSTID activity over Sutherland peaks in winter. Note that the occurrence rate of MSTIDs (shown by the red curve in Figure 2) is calculated as a ratio of the nights when MSTIDs were observed to the clear sky nights. Also shown in the figure is the confidence interval for the MSTID occurrence rate (red error bars) as there is some uncertainty on MSTID occurrence during nights with bad observation conditions. The minimum of the confidence interval is calculated from a ratio of number of nights with MSTIDs to the number of observation nights, that is, assumes that there were no MSTIDs during the bad observation nights. Assuming that MSTIDs were present in each of the bad observation nights, the maximum of the confidence interval was calculated as a ratio of sum of nights with MSTIDs and bad observation conditions to the number of observation nights. So for example, in December there were 25 observation nights, of which 12 had clear sky conditions and 13 bad observation conditions. From the 12 clear nights, MSTIDs were observed in 1 night. Therefore the MSTIDs occurrence rate is 1/12 = 0.08, with a confidence interval of [1/25 = 0.04, (1 + 13)/25 = 0.56].

Figure 3 shows the temporal distribution of the observed MSTID activity, where the vertical bar shows the time range of the single band (blue) and multi-band/periodic (red) MSTID observations. Note that multi-band

KATAMZI-JOSEPH ET AL. 4 of 20

and-conditions) on Wiley Online Library for rules of use; OA articles are governed by the applicable Crea

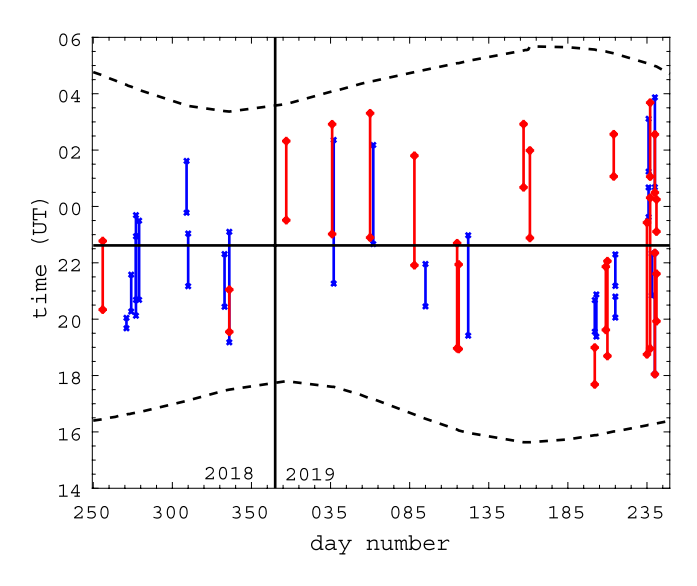


**Figure 3.** Observation time range of medium-scale traveling ionospheric disturbances (blue for single band and red for multi-band/periodic) between September 2018 and August 2019. Note that the black vertical and horizontal lines indicate day number 365 and local midnight, respectively, while the horizontal dashed black curves indicate sunset and sunrise times on the ground.

MSTIDs represent those that have more than a single wave front within the ASI field of view which propagate in a uniform direction. Figure 3 illustrates that the commencement of most of the MSTIDs (~67%) was prior to local midnight. The duration of the MSTID occurrence varied between approximately 22 min and 5 hr, with the majority of MSTIDs (~63%) having a duration that is less than 3 hr.

#### 3.1. Single Band Nighttime MSTIDs

The images in Figure 4 present an example of a single band nighttime MSTID structure, that is, dark band with the front aligned north-south. This figure presents a sample of background subtracted images taken on 2 May 2019 and projected on geographic coordinates. On this night ASI observations commenced around 1629 UT on 2 May and lasted until 3 May 0423 UT. The MSTID structure was observed moving westward in the ASI's field of view between roughly 1924 and 2258 UT.

Figure 5 presents north—south (N–S; top panel) and east—west (E–W; bottom panel) keograms of the 630.0 nm emission intensity for this night. In the E–W keogram the dark band can be seen at longitudes greater than  $\sim\!22^\circ$  between 19 and 22 UT, however no similar structure was seen in the N–S keogram. The slope of this dark band in E-W keogram is negative, implying the structure is propagating in the westerly direction. The speed of the MSTID was calculated from the slope of the structure in the E-W keogram using the linear least squares method, that is, finding the best linear fit to the keogram structure.

tures. The speed was determined to be  $\sim$ 48  $\pm$  6 m/s, while the propagation azimuth was computed to be 270° from the inverse tangent of the N-S and E-W speed components. The uncertainty in the speed calculation was

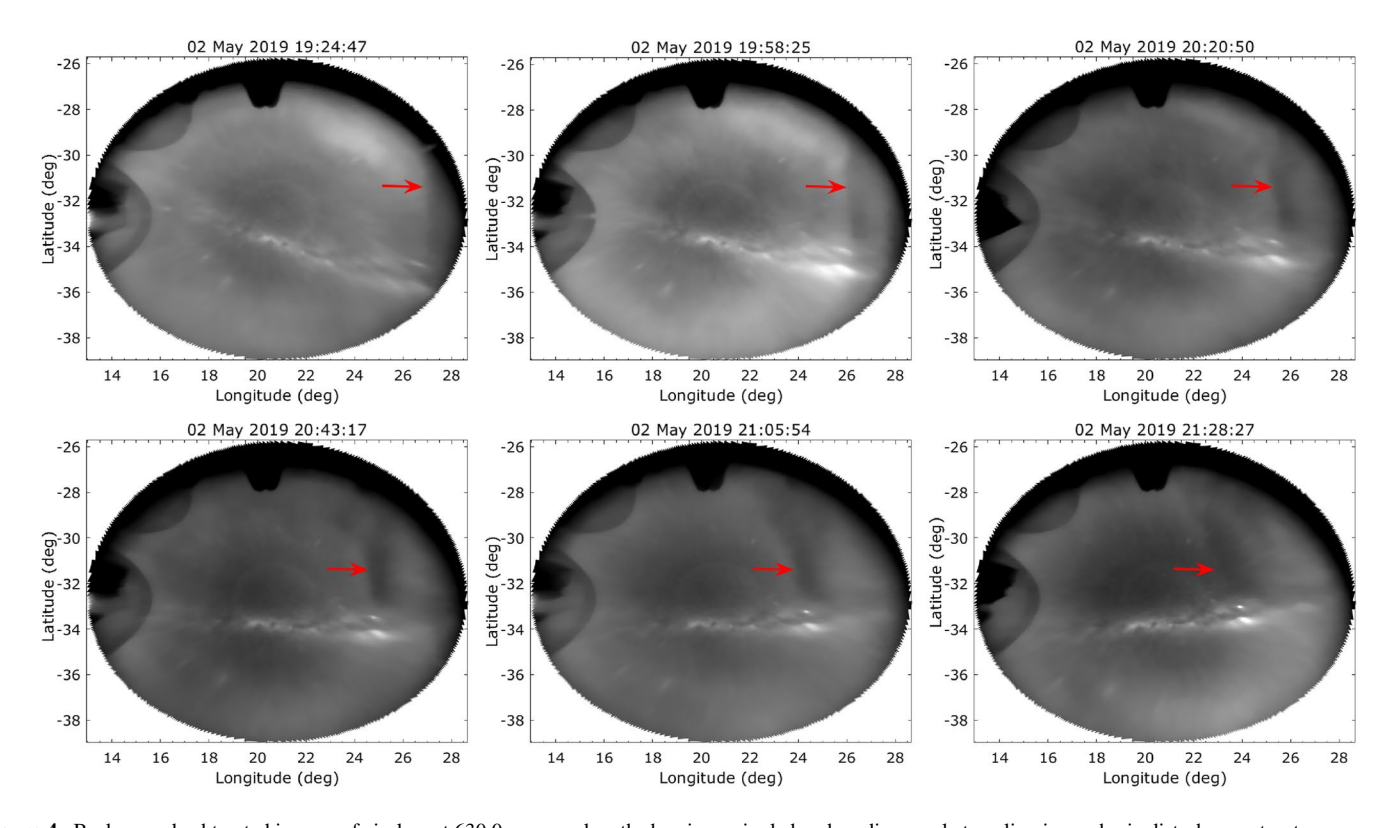


**Figure 4.** Background subtracted images of airglow at 630.0 nm wavelength showing a single band medium-scale traveling ionospheric disturbance structure (highlighted with a red arrow) on 2 May 2019. Note time is given in UT.

KATAMZI-JOSEPH ET AL. 5 of 20

2169902, 2022, 11, Downloaded from https://agupubs.onlinelbrary.wiley.com/doi/10.1029/2021A030375 by Boston University, Wiley Online Library on [23/06/2023]. See the Terms and Conditions (https://onlinelibrary.wiley.com/terms-and-conditions) on Wiley Online Library for rules of use. OA articles are governed by the applicable Centrity Common and Conditions (https://onlinelibrary.wiley.com/terms-and-conditions) on Wiley Online Library for rules of use. OA articles are governed by the applicable Centrity of Common and Conditions (https://onlinelibrary.wiley.com/terms-and-conditions) on Wiley Online Library for rules of use. OA articles are governed by the applicable Centrity of Common and Conditions (https://onlinelibrary.wiley.com/terms-and-conditions).

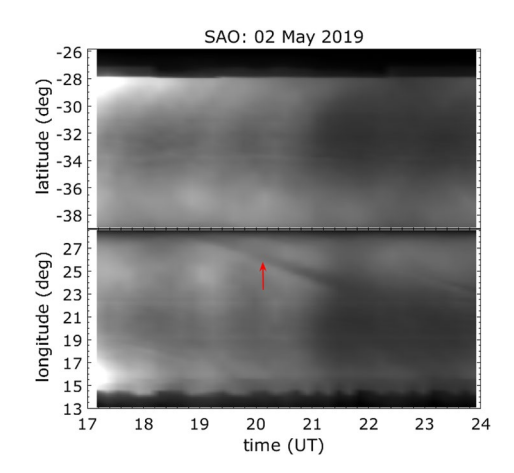


**Figure 5.** Keograms of 630.0 nm airglow emission intensity over Sutherland on 2 May 2019.

estimated from the uncertainty in the slope determination. Further analysis of the E-W keogram showed that the MSTID has spatial and temporal widths of  $\sim$ 74  $\pm$  19 km and  $\sim$ 30  $\pm$  6 min, respectively. The spatial and temporal widths were determined from the width of the dark band in space and time at various points and therefore represents a mean value while the uncertainty represents one standard deviation of the mean. Note that spatial and temporal widths are spatial and temporal scales, respectively, used to describe features of MSTIDs with only one wave front (i.e., single band MSTIDs), as opposed to wavelength and period which are distances in space and time, respectively, between two consecutive wave fronts of multi-band MSTIDs.

A total of 22 single band nighttime MSTIDs were observed in our data set, with the majority commencing pre-midnight (68%) and occurring during spring (36%) and winter (41%). These MSTIDs predominantly have a duration that is less than 2 hr (59%). The single band nighttime MSTIDs were found to travel in varied directions with speeds of 31–127 m/s, and had temporal as well as spatial scales of 11–30 min and 43–143 km, respectively. Figure 6 presents a distribution of single band nighttime MSTIDs' parameters with season, where the colors green, red, magenta and blue represent

spring, summer, autumn, and winter, respectively. In general, the majority of these MSTIDs had temporal scales of less than 30 min (90%) and spatial scales in the range of 50–100 km (64%). Single band nighttime MSTIDs with temporal scales greater than 30 min were only observed in autumn and winter, and those with spatial scales less than 50 km were only observed in spring and winter. Although the majority of the single band nighttime MSTIDs propagated west (59%), those observed during spring predominantly propagated between southwest and northwest directions. In addition, the majority of the observed single band nighttime MSTIDs had horizontal velocity less than 100 m/s (82%), a trend observed in all seasons.

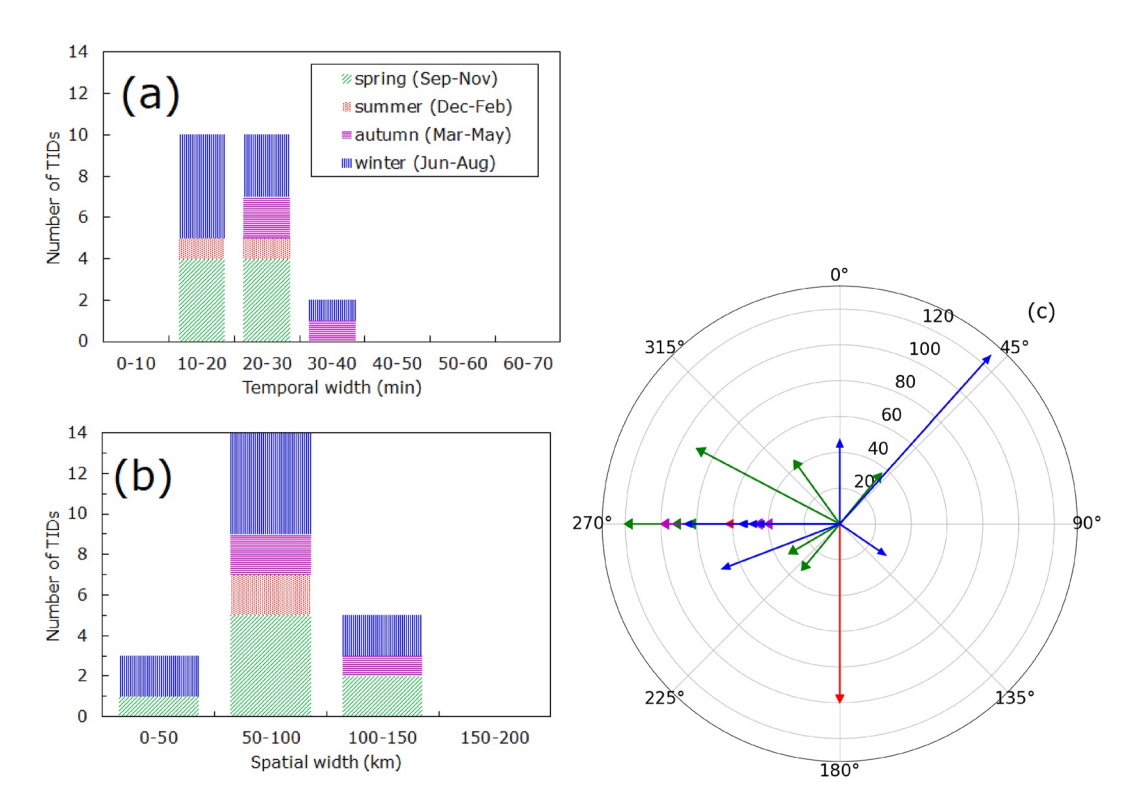


**Figure 6.** Distribution of single band nighttime medium-scale traveling ionospheric disturbances' temporal and spatial widths as well as propagation azimuth and speed with season. The colors green, red, magenta and blue represent spring, summer, autumn and winter, respectively.

KATAMZI-JOSEPH ET AL. 6 of 20

21699402, 2022, 11, Downloaded from https://agupubs.onlinelibrary.wiley.com/doi/10.1029/2022JA030375 by Boston University, Wiley Online Library on [23/06/2023]. See the Terms and Conditions

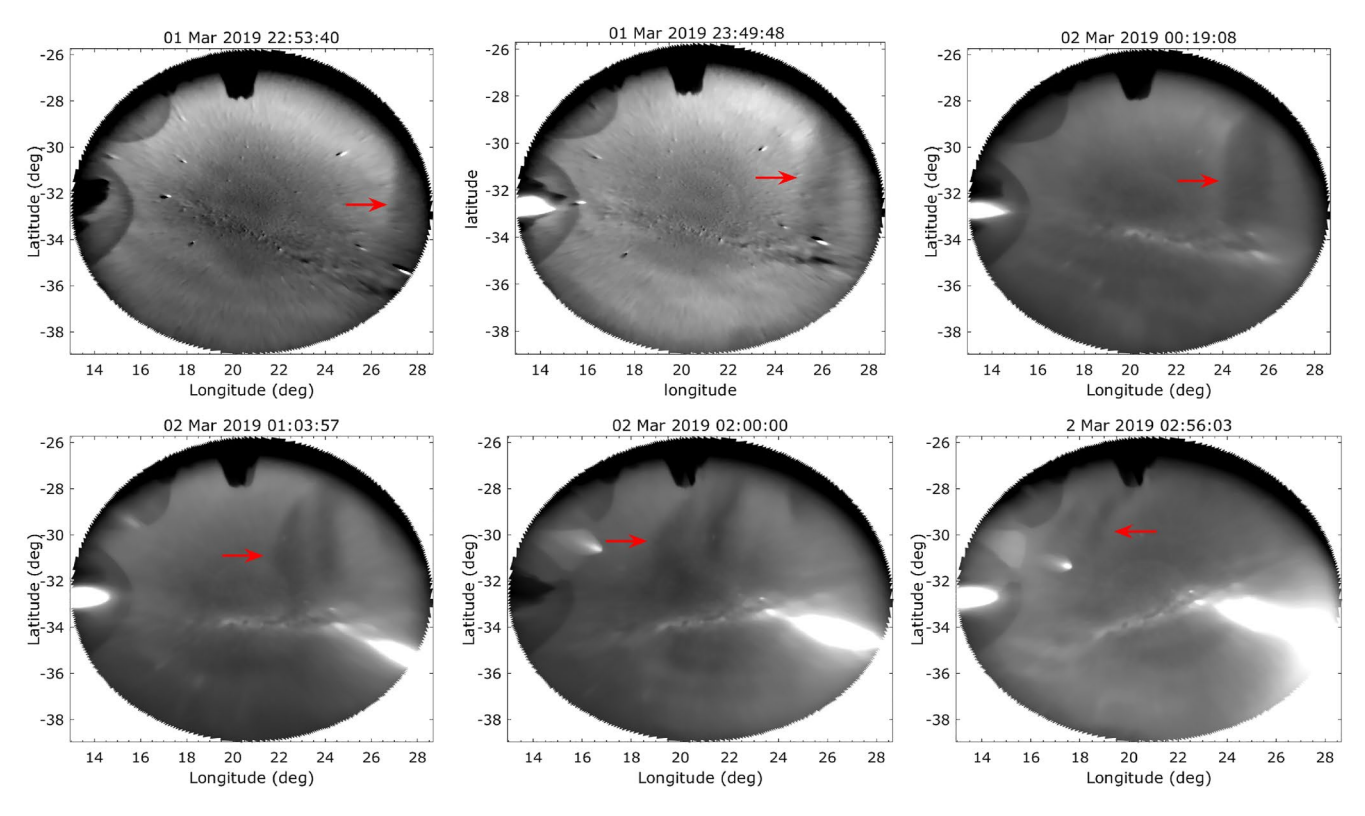
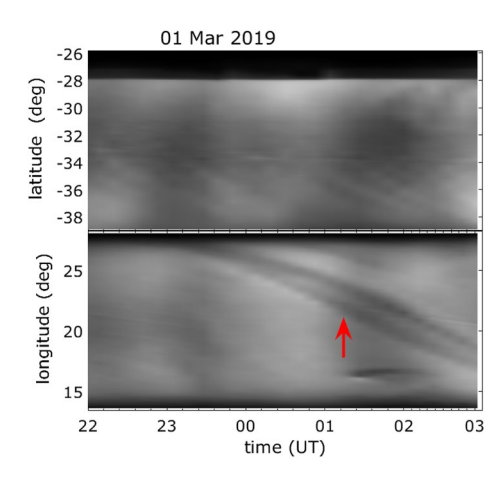


Figure 7. Background subtracted images of nighttime airglow at 630.0 nm wavelength showing a multi-band medium-scale traveling ionospheric disturbance structure (highlighted with a red arrow) on 1–2 March 2019.

#### 3.2. Multi-Band MSTIDs

The images presented in Figure 7 show an example of a multi-band MSTID structure that was observed on the night of 1 March 2019. During this night 630.0 nm airglow observations were made between 1801 and 0340 UT. Initially a single dark band structure that later resolved into a 2-band structure was observed from  $\sim$ 2231 UT until 0318 UT. Figure 7 shows a sample of images revealing the evolution of this structure as it propagates westward across the field of view of the ASI. The characteristics of this MSTID structure in terms of speed, azimuth, wavelength and period were  $\sim$ 91  $\pm$  2 m/s, 270°, 176  $\pm$  13 km, and 37  $\pm$  6 min, respectively as obtained



**Figure 8.** Keograms of 630.0 nm nighttime airglow emission intensity showing a multi-band medium-scale traveling ionospheric disturbance signature over Sutherland on 1–2 March 2019.

from the keograms shown in Figure 8. Note that the wavelength and period were independently determined from the keograms as the distances in space and time between the two consecutive bands of the MSTID structure, respectively. The velocity was again determined from the slopes of the dark bands in the keograms.

There were 21 multi-band (periodic) nighttime MSTIDs that were observed during this study, with the majority observed during winter (62%), while only 1 structure was observed during spring. Their dominant commencement time was almost evenly split between prior to midnight (52%) and post midnight (48%), but the majority were observed for longer than 2 hr (76%). These MSTIDs had periods and wavelengths of 26–155 min and 134–578 km, respectively. They propagated in varied directions with horizontal speeds in the range of 31–113 m/s, although almost all (95%) had speeds less than 100 m/s. Figure 9 presents a distribution of the MSTID's (a) period, (b) wavelength, (c) horizontal speed and propagation direction. In general, the most common MSTID periods are in the range of 40–70 min. The majority of the multi-band nighttime MSTIDs propagated westward (81%) in all seasons except spring when the only MSTID observed during this season propagated

KATAMZI-JOSEPH ET AL. 7 of 20

21699402, 2022, 11, Downloaded from https://agupubs.onlinelibrary.wiley.com/doi/10.1029/2022JA030375 by Boston University, Wiley Online Library on [23/06/2023]. See the Terms

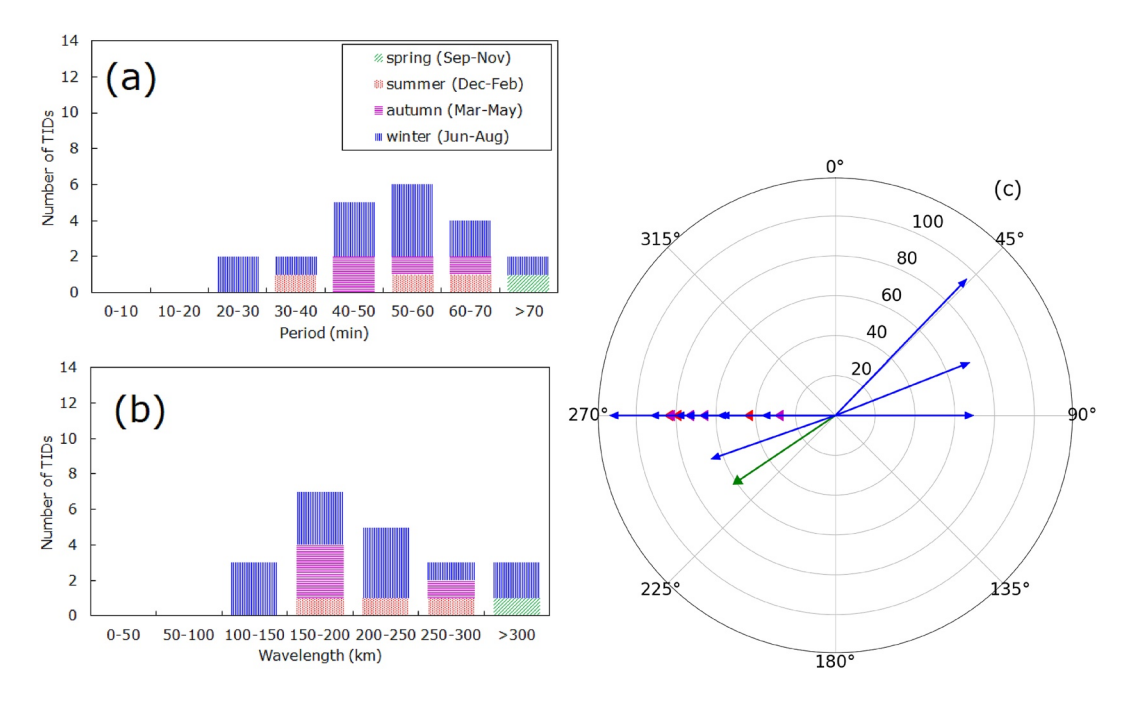


**Figure 9.** Distribution of (a) period, (b) wavelength, and (c) propagation azimuth and speed for multi-band medium-scale traveling ionospheric disturbances. Again the colors green, red, magenta, and blue represent spring, summer, autumn and winter, respectively.

southwest. Most of the observed multi-band nighttime MSTIDs had wavelengths less than 300 km (86%). However, those that were observed during autumn and winter are most likely to have wavelengths of 150–200 km and less than 250 km, respectively, while no other trends were detected during the other seasons. Similarly, the multi-band nighttime MSTIDs observed during winter were mostly likely to have periods of 40–60 min, but no trends were observed during the other seasons.

#### 3.3. Wind Filtering

The background neutral wind has a profound effect on the characteristics of propagating gravity waves in general, since gravity waves propagating in the direction of the wind with similar phase speeds will experience effects of Doppler shifting and possibly dissipation (Booker & Bretherton, 1967). The intrinsic frequency of a gravity wave under the influence of the background wind,  $\Omega$ , is given by:

$$\Omega = \omega - \vec{k} \cdot \vec{V} = \omega \left( 1 - \frac{v_z \cos \phi + v_m \sin \phi}{V_b} \right), \tag{1}$$

where  $\omega$  is observed frequency of the gravity wave,  $\vec{k}$  is the horizontal wave vector,  $\vec{V}$  is the horizontal wind velocity,  $v_z$  is the zonal component of the wind,  $v_m$  is the meridional component of the wind, and  $\phi$ , and  $V_h$  are the propagation azimuth and the horizontal phase velocity of the gravity wave, respectively (Cowling et al., 1971; Hines & Reddy, 1967; Yeh et al., 1972). This equation shows that if a gravity wave of a particular period and horizontal velocity propagates in the same direction and speed of the background neutral wind, the intrinsic frequency of the gravity wave shifts toward zero and the gravity wave loses its wave energy to the mean background flow. However, if the gravity wave propagates in a different direction to the background wind, it will be free from absorption. A polar plot, known as a blocking diagram, where radius and polar angle are given by the wave's phase velocity and propagation azimuth, respectively, shows critical level regions where propagation would be forbidden due to the background wind (i.e., regions where  $\Omega \to 0$  because  $v_z \cos \phi + v_m \sin \phi \to V_h$ ).

Figure 10 presents blocking diagrams for the months during which MSTIDs were observed in this study. Note that since wind measurements in August 2019 were only available for 2 nights due to instrument failure, a blocking diagram for this month was not produced. The red circles represent regions where propagation of a gravity wave, which might seed the MSTID, will be blocked by the background wind, that is, each circle represents the

KATAMZI-JOSEPH ET AL. 8 of 20

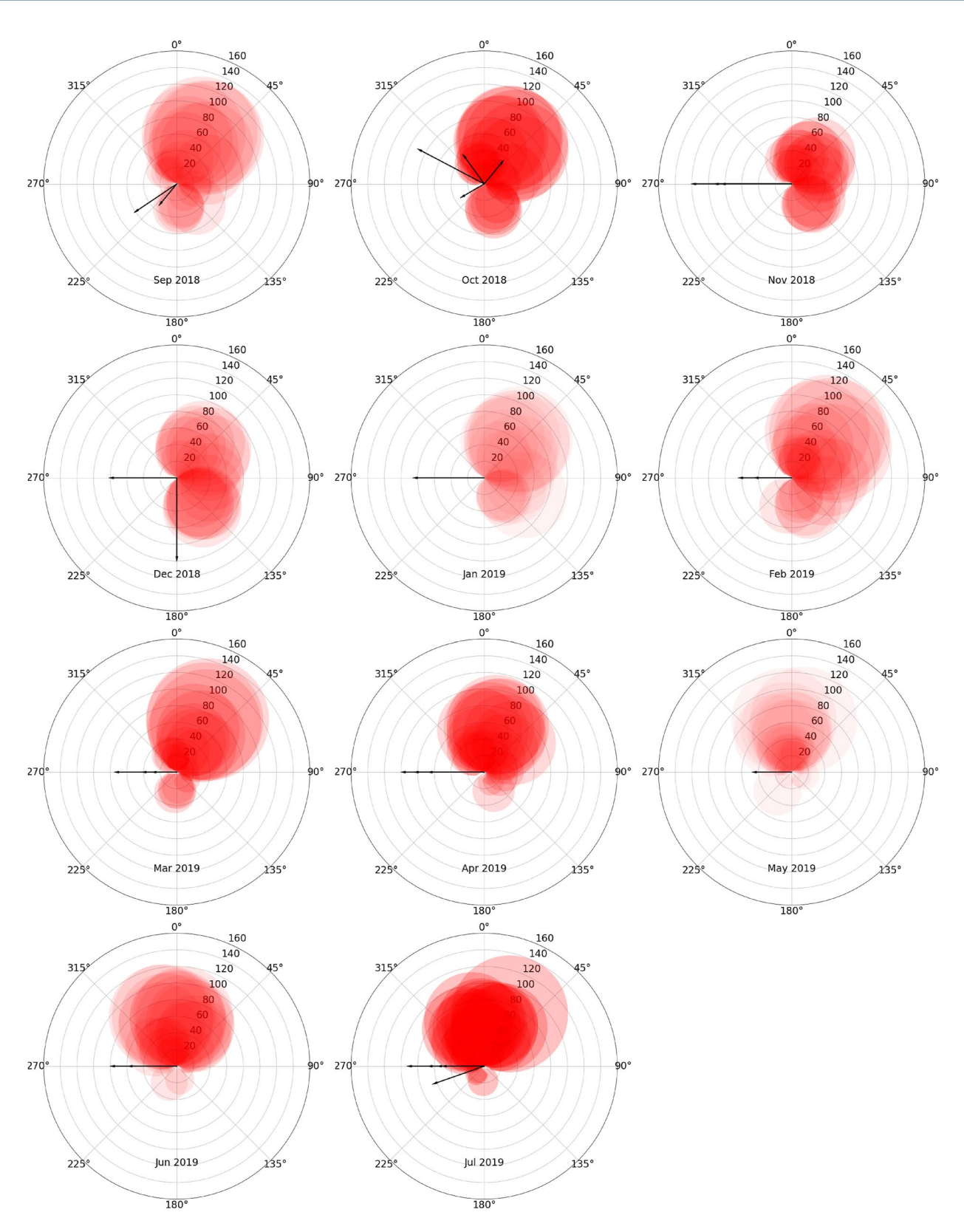


Figure 10. Blocking diagrams for monthly averaged Fabry-Perot interferometer measured neutral winds during the period of September 2018–July 2019.

KATAMZI-JOSEPH ET AL. 9 of 20

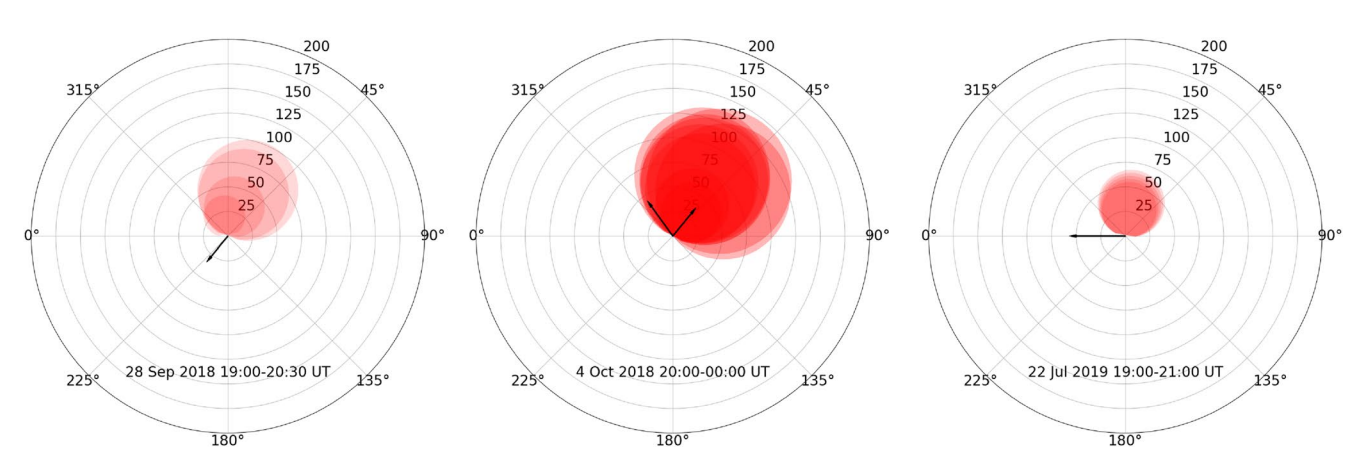


Figure 11. Blocking diagrams for medium-scale traveling ionospheric disturbance (MSTID) events on 28 September 2018, 4 October 2018, and 22 July 2019. Note that the blocking regions are determined from the wind conditions during the observation period of the MSTID events.

range of possible gravity wave velocity vectors that are equal to the wind velocity at each 30 min of the monthly averaged wind measurements by the FPI co-located with the ASI. Note that neutral wind data below the altitude where the MSTIDs exist would need to be considered in order to determine whether seeding gravity waves exist or not. However, such measurements do not exist over our region of interest. In the construction of the blocking regions (red circles), we used gravity wave velocity range of 0–400 m/s and 0–360° (i.e.,  $V_b$  and  $\phi$ , respectively, in Equation 1), corresponding to typical reported gravity wave propagation characteristics. The results in Figure 10 show that the blocking regions are mostly between north-west and south-west directions, with the west direction being largely free/clear. This may explain why most of the observed MSTIDs propagated westward. However, although the majority of the observed MSTIDs propagate outside the forbidden regions, indicating that they had unrestricted propagation, there are several events that propagate within the forbidden region (e.g., some MSTIDs in September, October and July). To find out if this was due to using averaged wind when calculating the blocking region, further investigation of these events was done where the wind data from the same nights as the MSTID observations were used to generate the blocking diagrams. Results for these events are shown in Figure 11 and they show that while the wind conditions on 28 September 2018 and 22 July 2019 allowed for unrestricted propagation of the observed MSTIDs, this was not the case for those observed on 4 October 2018. This latter event therefore requires further investigation.

#### 3.4. Sporadic E and Spread-F Influence

Figure 12 presents an example of simultaneous observations of MSTIDs with sporadic E and spread-F, which occurred on 8 January 2019. On this night a multi-band MSTID was observed propagating west between 0017 and 0219 UT. Within the same time period, intermittent sporadic E and spread-F were recorded by the three ionosondes located within the field of view of the imager. The critical frequency of sporadic E (foEs) varied between 1.48 and 4.17 MHz on this night. Ionosonde data was surveyed to investigate concurrent occurrences of MSTIDs and sporadic E as well as spread-F. The results of this analysis are presented in Table 2 and Figure 13. Note that the Louisvale station had missing data from February to August 2019, and the Grahamstown station was missing data for some events in November, December 2018 and July 2019 (see Table 2). Also note that for only 9 out of the 43 observed MSTIDs were ionosonde measurements from all three ASI neighboring stations available. All except one (i.e., 8) of these 9 propagated westward or had a western component to their propagation and the majority are single band MSTIDs. From these 8 events, 4 were observed when sporadic E, which varied between 1.2 and 4.2 MHz, was also recorded in all three ionosonde stations, and 6 were observed simultaneously with sporadic E occurrence over at least one station. On the other hand, 5 out of these 8 MSTIDs were observed simultaneously with spread-F in at least one ionosonde station while 3 MSTIDs were observed with spread-F recorded over all three ionosonde stations.

Figure 13 presents the percentage of the 43 detected MSTIDs that were observed concurrently with sporadic E and/or spread-F over all 3 stations, at least 2 stations and at least 1 station. From this figure it can be seen that in general the majority of detected MSTIDs were observed simultaneously with sporadic E (65%) and spread-F

KATAMZI-JOSEPH ET AL. 10 of 20

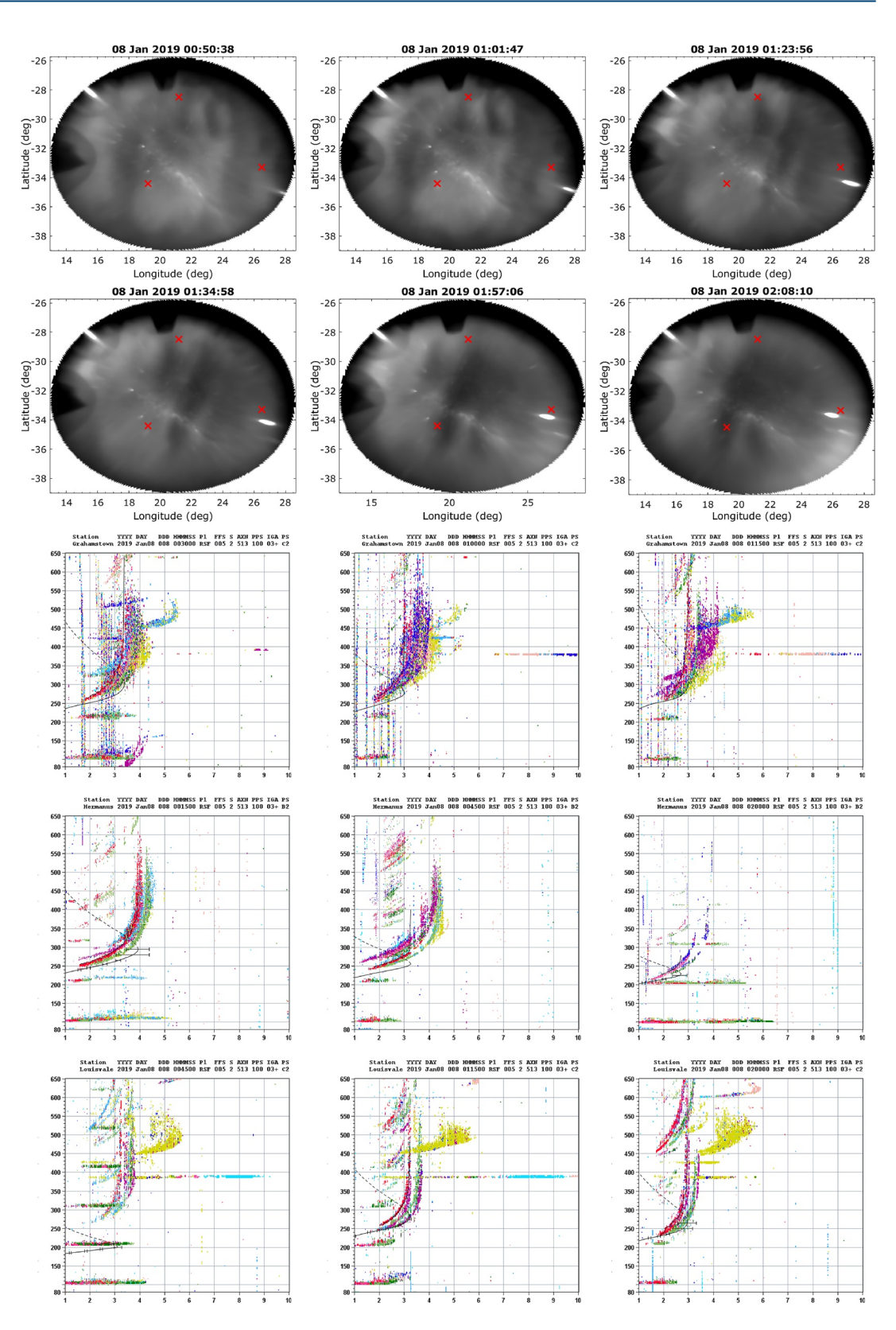


**Figure 12.** Images and ionograms showing medium-scale traveling ionospheric disturbance events and sporadic E and/ or spread-F occurrences over Grahamstown, Hermanus, and Louisvale on 8 January 2019. The red crosses in the images mark the location of the ionosondes. The *x* and *y* axes of the ionograms represent frequency (MHz) and virtual height (km), respectively.

KATAMZI-JOSEPH ET AL. 11 of 20

2169402, 2022, 11, Dowloaded from https://agupubs.onlinelibrary.wiley.com/doi/10.1092/0221A030375 by Boston University, Wiley Online Library on [23:06/2023]. See the Terms and Conditions (https://onlinelibrary.wiley.com/terms-end-conditions) on Wiley Online Library for rules of use; OA articles are governed by the applicable Cerative Communications.

 Table 2

 Presence of Sporadic E and Spread-F on Nights of Observed Medium-Scale Traveling Ionospheric Disturbance Events

Date	Time	Sporadic E			Spread-F			Propagation	Band
	UT	GR13L	HE13N	LV12P	GR13L	HE13N	LV12P	Direction	Type
13 September 2018	2020–2246	No	Yes	Yes	No	No	No	SW	Multi
28 September 2018	1940-2002	No	No	No	No	No	No	SW	Single
01 October 2018	2016–2134	No	No	No	No	Yes	No	SW	Single
04 October 2018	2007-2341	Yes	Yes	Yes	Yes	Yes	Yes	NE	Single
04 October 2018	2041-2256	Yes	Yes	Yes	Yes	Yes	Yes	NW	Single
06 October 2018	2041–2329	Yes	Yes	Yes	Yes	Yes	Yes	NW	Single
05 November 2018	2346-0136	Yes	Yes	Yes	No	No	No	W	Single
06 November 2018	2110-2302	No	Yes	No	No	No	Yes	W	Single
29 November 2018	2026–2218	_	Yes	Yes	_	No	No	W	Single
02 December 2018	1910–2306	_	Yes	Yes	_	No	Yes	W	Multi
02 December 2018	1933–2102	-	Yes	Yes	-	No	Yes	S	Single
07 January 2019	2330-0219	Yes	Yes	Yes	Yes	Yes	Yes	W	Multi
05-06 Feb 2019	2301-0255	No	Yes	_	No	Yes	_	W	Single
06-07 February 2019	2115-0221	No	Yes	_	No	Yes	_	W	Multi
01-02 March 2019	2253-0318	Yes	YES	_	No	No	_	W	Multi
03-04 March 2019	2239-0210	Yes	No	_	Yes	Yes	_	W	Single
29-30 March 2019	2154-0147	No	No	_	No	No	_	W	Multi
05 April 2019	2027–2157	Yes	No	_	No	No	_	W	Single
25 April 2019	1857-2241	Yes	Yes	_	Yes	Yes	_	W	Multi
26 April 2019	1856–2156	No	Yes	_	No	Yes	_	W	Multi
02 May 2019	1924–2258	No	No	_	No	No	_	W	Single
07 June 2019	0040-0255	No	No	_	Yes	No	_	W	Multi
10 June 2019	2252-0159	No	Yes	_	Yes	Yes	_	W	Multi
21 July 2019	1741–1859	_	Yes	_	_	Yes	_	W	Multi
21 July 2019	1933-2040	_	Yes	_	_	Yes	_	W	Single
22 July 2019	1922–2052	No	Yes	_	Yes	Yes	_	W	Single
28 July 2019	1937–2151	No	No	_	Yes	Yes	_	W	Multi
29 July 2019	1841-2203	No	Yes	_	Yes	Yes	_	W	Multi
03 August 2019	0103-0233	No	No	_	No	No	_	W	Multi
03 August 2019	2003-2048	No	Yes	_	No	No	_	W	Single
03 Aug 2019	2110-2217	No	No	_	No	No	_	W	Single
23 August 2019	1845–2122	Yes	Yes	_	Yes	Yes	_	W	Multi
24-25 August 2019	2337-0040	No	No	_	No	Yes	_	N	Single
25 August 2019	0114-0306	No	No	_	Yes	Yes	_	W	Single
25 August 2019	1857-0018	No	No	_	Yes	Yes	_	W	Multi
26 August 2019	0130-0340	No	No	_	Yes	Yes	_	Е	Multi
26 August 2019	2050–2219	No	No	_	Yes	Yes	_	NE	Single
28 August 2019	1802–2157	No	Yes	_	No	No	_	SE	Single
28 August 2019	1802–2221	No	Yes	_	No	No	_	NE	Multi
29 August 2019	0029-0233	No	Yes	_	Yes	Yes	_	W	Single
29 August 2019	0040-0330	No	Yes	_	Yes	Yes	_	W	Multi

KATAMZI-JOSEPH ET AL. 12 of 20

Table 2 Continued									
	Time	Sporadic E			Spread-F			Propagation	Band
Date	UT	GR13L	HE13N	LV12P	GR13L	HE13N	LV12P	Direction	Type
29 August 2019	1955–2136	No	No	-	Yes	Yes	_	W	Multi
29-30 August 2019	2306-0014	No	No	_	No	Yes	_	Е	Multi

(72%) over at least one station. However, the number reduces significantly for simultaneous observations of TIDs and sporadic E or spread-F over all 3 stations; 12% and 9% for MSTID with sporadic E and MSTID with spread-F, respectively. Table 2 reveals that of the MSTIDs that are observed simultaneously with sporadic E occurrence over at least one station (28 out of 43), 24 (86%) have a westerly propagation. Also, only 2 MSTIDs are not observed simultaneously with local sporadic E at all and both propagate southwest. Furthermore, 13 of the MSTIDs that were observed concurrently with sporadic E are of the multi-band type, while 15 are of the single band structures. Of the 30 MSTIDs that were observed concurrently with spread-F events 16 are multi-band and 14 are single band structures.

#### 4. Discussion

Note. "-" represent no data.

Nighttime MSTIDs were observed in ASI images as single or multi-band structures in roughly equal measure over South Africa during September 2018-August 2019. Observations of single band structures are not that common as most optical studies of nighttime MSTIDs report predominantly wave-like structures consisting of alternating dark and bright bands (e.g., Huang et al., 2016; Kubota et al., 2011; Makela et al., 2010; Narayanan et al., 2014, 2018; Otsuka et al., 2004, 2007; Rajesh et al., 2016; Shiokawa et al., 2003, 2009), with relatively fewer studies reporting dark band structures (e.g., Amorim et al., 2011; Candido et al., 2008; Figueiredo et al., 2018; Martinis et al., 2011; Pimenta, Kelley, & Candido, 2008; Pimenta, Kelley, et al., 2008; Rathi et al., 2021). In fact, a study by Figueiredo et al. (2018) on nighttime MSTIDs over Brazil reported many more observations of periodic MSTIDs compared to dark band structures. What is unique about the dark band structures reported here is that many do not span the entire field of view of the ASI, for example, see Figures 4 and 7. For example, the widths of the single band MSTIDs reported here did not exceed 143 km, while Candido et al. (2008) and Figueiredo et al. (2018) reported that they observed low latitude MSTIDs with widths (zonal extensions) that exceeded 1000 km over Cachoeira Paulista in Brazil. Furthermore, Figueiredo et al. (2018) found the morphology and characteristics of their single band and periodic nighttime MSTIDs to differ, and as a result attributed their generation through different processes. They concluded that single band MSTIDs were generated through ionospheric instability linked to electrodynamic coupling between the E and F layers, while the periodic MSTIDs were attributed to propagation of gravity waves. Similarly, Rathi et al. (2021) concluded that the periodic and dark band MSTIDs they observed on 02 October 2019 over Hanle, India were seeded by gravity waves and E-F coupling, respectively. However, in this study the characteristics of the majority of both single band and multi-band MSTIDs were similar, which suggests their generation mechanism may be the same. This seems to be supported by literature where studies that have reported on observations of either periodic/multi-band MSTIDs or dark band MSTIDs have proposed the same generation mechanism, that is, coupled electrodynamic processes seeded by neutral wind, sporadic E and/or gravity waves (e.g., Amorim et al., 2011; Candido et al., 2008; Huang et al., 2016; Makela et al., 2010; Martinis et al., 2011; Otsuka et al., 2004, 2007; Pimenta, Kelley, & Candido, 2008; Pimenta, Kelley, et al., 2008; Rajesh et al., 2016; Shiokawa et al., 2003).

The general analysis of the MSTID parameters presented in this study show that the nighttime MSTIDs over Sutherland have similar characteristics to those observed in other midlatitude 630.0 nm airglow measurements. For example, the MSTIDs in this study commenced mostly during the premidnight period, in agreement with Kubota et al. (2011) and Fukushima et al. (2012) who also reported that most of the nighttime MSTIDs occurred premidnight over Alaska and Kotatabang (Indonesia) respectively. Similarly, Shiokawa et al. (2003, 2005, 2006) found that the occurrence rate peaked in the premidnight and decreased postmidnight for nighttime MSTIDs over Indonesia, Japan and Australia. The nighttime MSTIDs presented here had velocities in the range of 30–127 m/s, in agreement with a reporting of a 50–170 m/s range for those observed over Puerto Rico by Garcia et al. (2000),

KATAMZI-JOSEPH ET AL. 13 of 20

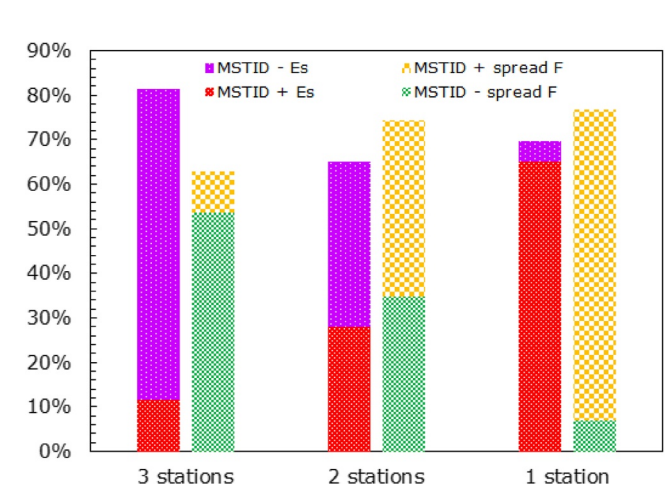


**Figure 13.** Probability of simultaneous observations of medium-scale traveling ionospheric disturbances and sporadic E and/or spread-F during the period of September 2018 to August 2019.

as well as 30-150 and 50-150 m/s reported by Narayanan et al. (2014) and Huang et al. (2016) and Huang et al. (2018) for nighttime MSTIDs over Japan and China, respectively. However, the speeds reported here are slightly lower than those reported by Martinis et al. (2019) for MSTID events they observed over Sutherland, which had speeds of 93-168 m/s. Periods calculated here were also comparable to those determined by Kubota et al. (2011), and Huang et al. (2016, 2018) who reported ranges of 15-60 min and 0.5-1.5 hr (30–90 min), respectively, compared to a range of 26–155 min reported in this study, with the majority (90%) having periods less than 70 min. We observed nighttime MSTIDs having wavelengths of 134-578 km, although the majority (86%) had wavelengths of 100-300 km. The latter range is in agreement to those obtained from Garcia et al. (2000); Shiokawa et al. (2003) and Rajesh et al. (2016) who reported ranges of 100-250 km, 100-300 km and 150-300 km respectively for nighttime MSTIDs at similar latitudes. Lastly, the majority of the observed MSTIDs, but not all, were accompanied by spread-F. This means that there isn't necessarily a 1 to 1 correspondence between MSTID and spread-F occurrence. This results was also found by Narayanan et al. (2018). However, Shiokawa et al. (2003) showed very low correspondence of MSTID and spread-F occurrences. The low concurrent occurrence reported by Shiokawa et al. (2003) could be related to limited

ionosonde resolution (their ionosonde data had 1 hr resolution while ours have 15 min) as spread-F structures are intermittent, which could result in the underestimation of concurrent MSTID and spread-F event.

The nighttime MSTIDs reported here mainly propagated westward. This observation is dissimilar to the northwest propagation direction for southern hemisphere nighttime MSTIDs generated through the Perkins instability reported by Otsuka et al. (2004), Shiokawa et al. (2005), Martinis et al. (2011) and Narayanan et al. (2018). However, Martinis et al. (2019) argued that this instability could still be responsible for even westward propagating nighttime MSTIDs. In that study, they investigated a few nighttime MSTID events detected over conjugate stations in Sutherland and Asiago (Italy). MSTIDs propagated in the expected southwest direction in Italy. However, their propagation was westward over Sutherland. They reasoned that since the nighttime MSTIDs generated through Perkins instability seeded by the electrodynamical coupling of the sporadic E and F regions are known to occur simultaneously in both hemisphere, theirs were also electrified MSTIDs. The westward propagation direction over Sutherland was justified as being within the efficient propagation direction for Perkins instability associated structures. This is because the Perkins instability's linear growth maximizes when the MSTID wave vector is between magnetically west and the ionospheric current. Since Sutherland is at magnetic declination of 24°W, propagation will fall within the azimuthal direction of 246°–336° which can be unstable for the Perkins instability, although the direction of ionospheric current also contributes.

The study reported here shows for the first time that the background wind over Sutherland restricts propagation in most directions except the west as illustrated by the blocking diagrams presented in Figure 10, thus supporting the westward propagation of the MSTIDs observed in this study and reported by Martinis et al. (2019). The Perkins instability growth rate ( $\gamma$ ) is expected to maximize when the meridional component ( $\nu_m$ ) is northward (positive) and the zonal component ( $\nu_z$ ) is eastward (positive) over Sutherland where the magnetic inclination/dip angle (D) is  $\sim$ -65° and the magnetic declination angle ( $\delta$ ) is  $\sim$ -24°, since (Duly et al., 2013; Garcia et al., 2000; Narayanan et al., 2018):

$$\gamma_{\text{max}} \propto v_z \sin D \sin \delta + u_z \cos \delta - v_m \sin \delta - v_m \sin D \cos \delta.$$
 (2)

This was mostly the case, especially premidnight (when most of the MSTIDs reported here are observed), according to the wind observations presented in Figure 14 as obtained from the imager co-located FPI. Note that the winds shown here are monthly averages illustrating the general wind characteristics during the period of our study. There are of course months where the wind conditions were not favorable in terms of Perkins instability, such as May–July 2019 where the meridional wind was southward (poleward) even though the zonal wind was still eastward. In these months, the MSTIDs could have formed because of the combined effects of the coupled sporadic E and wind in the opposite hemisphere, as illustrated by Narayanan et al. (2018), or gravity wave activity. In fact, Narayanan et al. (2018) reported that poleward wind, as the case in the period of May–July 2019

KATAMZI-JOSEPH ET AL. 14 of 20

21694042, 2022, 11, Downloaded from https://agupubs.onlinelibrary.wiley.com/doi/10.1029/2021/A030375 by Boston University, Wiley Online Library on [23906/2023]. See the Terms and Conditions (https://onlinelibrary.wiley.com/terms-and-conditions) on Wiley Online Library for rules of use; OA articles are governed by the applicable Creative Commons Licenseity.

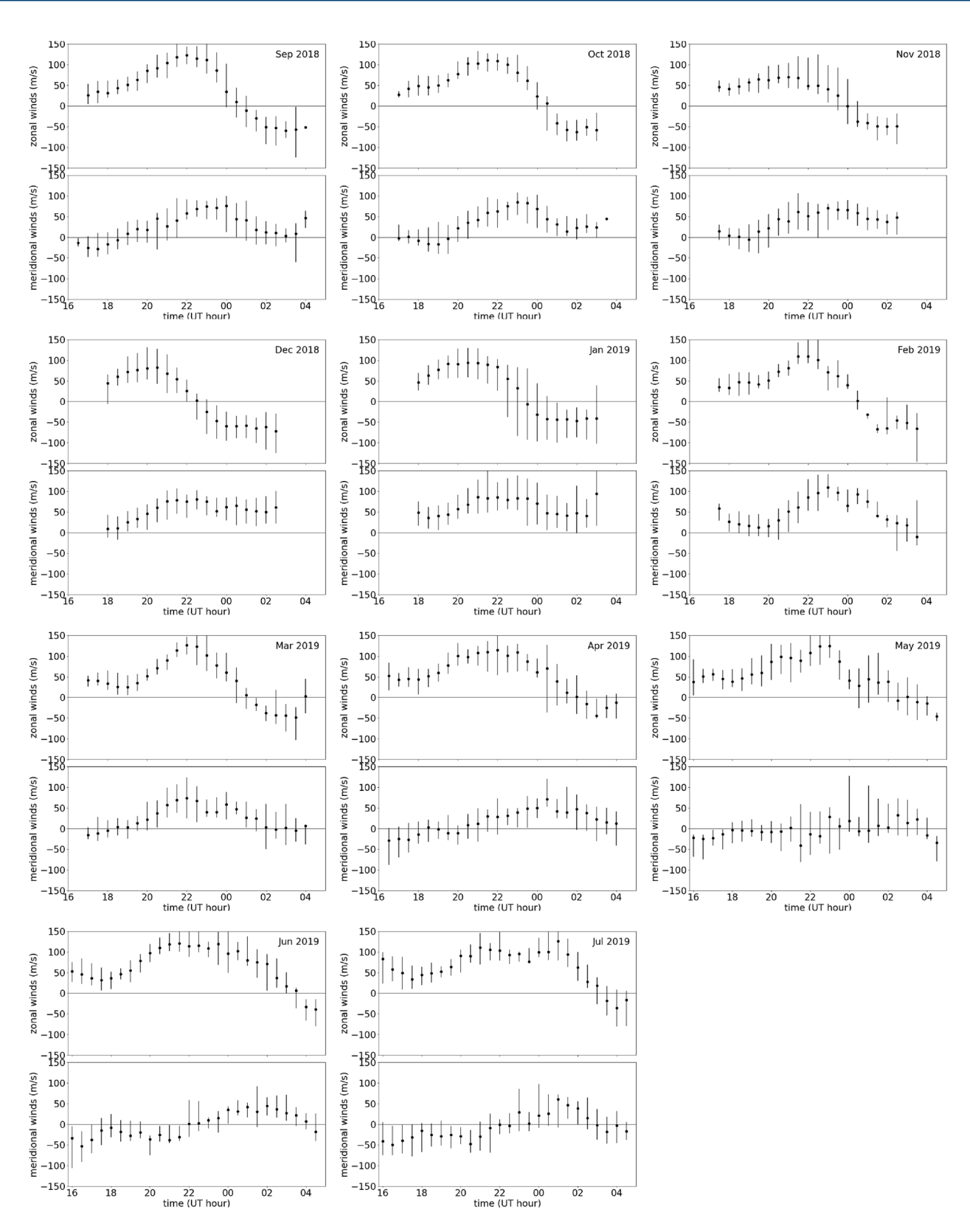
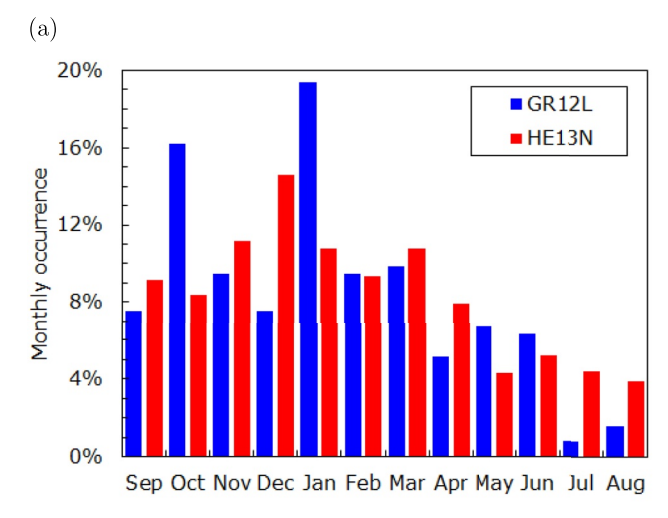


Figure 14. Fabry-Perot interferometer monthly averaged thermospheric zonal and meridional wind measurements over Sutherland for the period September 2018–July 2019.

KATAMZI-JOSEPH ET AL. 15 of 20

21699402, 2022, 11, Downlo.

onlinelibrary.wiley.com/doi/10.1029/2022JA030375 by Boston University, Wiley Online I



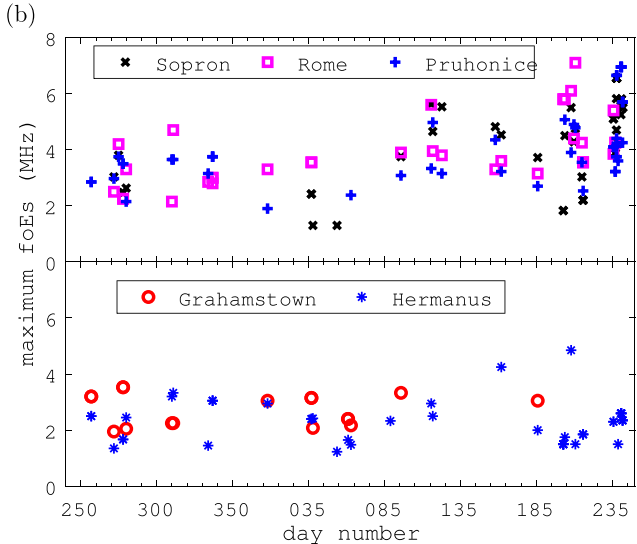


**Figure 15.** (a) Monthly occurrence of nighttime sporadic E region over Grahamstown and Hermanus and (b) maximum nighttime frequency of sporadic E over for period of September 2018–August 2019.

in this study, reduces amplitudes of MSTIDs due to the wind lowering the plasma to enhanced recombination and/or increased Pedersen conductivity altitudes. This meridional wind influence could be explored further for our MSTIDs in a future study.

The influence of sporadic E in amplifying the Perkins instability responsible for electrified MSTIDs can be further supported by the fact that its variability peaks during the summer solstice in both hemisphere (e.g., Arras et al., 2008; Haldoupis et al., 2007; Wu et al., 2005). This seasonal variation is also observed in the South African region as seen in Figure 15a which shows typical nighttime occurrence, in monthly percentage, of sporadic E using measurements from the Grahamstown and Hermanus ionosondes. Furthermore, the majority of the MSTIDs reported in this study were associated to sporadic E, similar to observations by Bowman et al. (1994), Kelley et al. (2003), and Paznukhov et al. (2020). However, the maximum foEs during the majority of these events (74%) was less than 4 MHz, whereas Narayanan et al. (2018) reported that the electrified MSTIDs are generated when foE is greater than 6 MHz in at least one hemisphere, while Sivakandan et al. (2022) observed that the onset of their MSTIDs coincided with sporadic E which had foEs greater than 4 MHz. Considering the lower foEs intensity over South Africa, it is possible that the nighttime MSTIDs reported here were affected by the sporadic E at the conjugate point in the northern hemisphere. The conjugate station in Asiago, Italy (45.9°N, 11.5°E; magnetic latitude: 40.7°), has no co-located ionosonde station, therefore we checked nighttime Es activity from ionosondes in close proximity to Asiago, namely Sopron (47.6°N, 16.7°E), Rome (41.9°N, 12.50°E) and Pruhonice (50.0°N, 14.6°E). The results are presented in Figure 15b which shows maximum nighttime foEs prior to and during the time of detected MSTIDs occurrence over ionosondes in the southern hemisphere (Grahamstown and Hermanus; bottom panel) and northern hemisphere (Sopron, Rome, and Pruhonice; top panel). We found that all but one of the MSTIDs reported here (i.e., 98%) were accompanied by Es activity in at least one hemisphere. However, only 54% and 17% of the observed MSTIDs were accompanied by Es with critical frequency over 4 and 6 MHz in at least one hemisphere, respectively. In fact, some of the MSTIDs were accompanied with Es that had maximum frequency as low as 1.3 MHz. This suggests that the thresholds found by Narayanan et al. (2018) and Sivakandan et al. (2022) may not apply universally. Note that for the majority of MSTIDs observed at Sutherland in this study, the conjugate station in Asiago, Italy, is cloudy. Therefore, an extension to the Martinis

et al. (2019) study was not attempted. However, there are 10 potential conjugate cases from the events reported here that require further investigation for a future study.

In terms of monthly nighttime MSTID occurrences, this study revealed that these wave-like disturbances peaked near the southern winter solstice period (i.e., May–August), where the occurrence rate is on average ~3 times greater compared to other seasons. This result is in agreement with observations from other longitudinal sectors in the southern hemisphere obtained using optical and radio instruments (e.g., Fukushima et al., 2012; Rajesh et al., 2016; Shiokawa et al., 2006). It should be noted that in the Euro-Africa longitude sector, a contradictory seasonal occurrence pattern is reported. This study reports a southern winter peak which agrees with Kil and Paxton (2017) at similar region but over Europe, Kotake et al. (2006) and Otsuka et al. (2013) reported primary peaks during the northern winter solstice (December), while Hernandez-Pajares et al. (2006) and Kil and Paxton (2017) reported primary peaks during the northern summer solstice (June). Nonetheless, these studies illustrate that the solstices occurrence peaks are consistent in both the southern and northern hemispheres. Rajesh et al. (2016) and Kil and Paxton (2017) suggested that the solstices peak occurrence may be due to the dominant effect of the sporadic E in the summer hemisphere generating MSTIDs in both hemispheres through interhemispheric coupling (Otsuka et al., 2004). Whereas Kotake et al. (2007) and Shiokawa et al. (2003) explained the

KATAMZI-JOSEPH ET AL. 16 of 20



Acknowledgments

This work is based on the research supported wholly/in part by the National

Research Foundation of South Africa

(Grant: 148779). ZKJ acknowledges support from the Fulbright Program (Grant: PS00285598). Work at the University of Illinois was supported by

the National Science Foundation through

Grant AGS-16-51298, CM acknowledges support from CEDAR NSF Grant

#1552301 and Aeronomy NSF Grant

## **Journal of Geophysical Research: Space Physics**

10.1029/2022JA030375

solstices peaks in nighttime MSTID occurrence in the following manner. The solstices peak of the nighttime MSTIDs is inversely proportional to the neutral density, which peaks during the equinoxes and is at minimum during the solstices (Fuller-Rowell, 1998). Since the amplitudes of gravity waves are large when the neutral density is low and large AGWs can cause large plasma disturbances such as MSTIDs (Hines, 1960), it is possible that the seasonal MSTID occurrence could be linked to that of neutral density. Also, neutral density has another link to the seasonal nighttime MSTID occurrence variation through the Perkins instability since the linear growth rate of this instability is also inversely proportional to the neutral density. The latter gives additional support to Perkins instability as the possible mechanism through which the majority of the MSTIDs observed here, primarily those that propagated westward, were generated. The remaining MSTIDs events, that is, those with characteristics that are not supported by electrodynamic processes, may be have been seeded by gravity waves similar to Kubota et al. (2011), but further investigations are needed to support this.

#### 5. Conclusion

This study presented the first general characteristics of nighttime MSTIDs over South Africa, using 630.0 nm airglow measurements from an ASI in Sutherland. These MSTIDs were comprised, in almost equal measure, of single and multi-band structures that were observed during the period of September 2018-August 2019. We found that the nighttime MSTIDs in this region had the following characteristics:

- Wavelength of 134-578 km,
- Spatial width of 43–143 km,
- Period of 26-155 min,
- Temporal scale of 11–30 min,
- Speeds of 31–127 m/s,
- Propagated mostly westward, which was found to be the direction least restricted by the background neutral wind as well as within the Perkins instability's favored propagation azimuthal range.

The occurrence of individual nighttime MSTID was seen at all times throughout the night and seasons but most were observed before midnight and near southern winter solstice, consistent with observations in other longitudinal sectors. A relationship between occurrences of the nighttime MSTIDs, sporadic E and spread-F was investigated and it was found that the majority of the nighttime MSTIDs had occurrence correlation with both sporadic E and spread-F. Observations also revealed that sporadic E occurrence peaked during the summer solstice, in agreement with global sporadic E observations. The seasonal variations of the MSTID and sporadic E occurrences as well as the favored propagation of the MSTIDs and equator-eastward direction of the background wind suggested that the Perkins instability, under the seeding of sporadic E and/or neutral wind, may be the likely dominant source of nighttime MSTIDs reported on in this study with gravity waves as a potential supplementary/ additional seeding mechanism.

As a future study, optical data from several years may help us establishment whether there are distinguishing characteristics of single band and multi-band MSTIDs. In addition, interhemispheric coupling could be explored further in a MSTID study that involves long-term data from both Sutherland and its magnetic conjugate Asiago, Italy.

### **Data Availability Statement**

Sutherland ASI and FPI data are available at http://sirius.bu.edu/dataview/ and http://airglow.ece.illinois.edu/ Data/Calendar, respectively, while ionosonde data are available through GIRO's DIDBase (https://ulcar.uml.edu/ DIDBase/). The sunset and sunrise times were obtained from https://www.esrl.noaa.gov/gmd/grad/solcalc/.

### References

Amorim, D. C. M., Pimenta, A. A., Bittencourt, J. A., & Fagundes, P. R. (2011). Long-term study of medium-scaletraveling ionospheric disturbances using OI 630 nm all-sky imaging and ionosonde over Brazilian low latitudes. Journal of Geophysical Research, 116(A6), A06312. https://doi.org/10.1029/2010JA016090

Arras, C., Wickert, J., Beyerle, G., Heise, S., Schmidt, T., & Jacobi, C. (2008). A global climatology of ionospheric irregularities derived from

#2152365. JB acknowledges support from CEDAR NSF Grant #1552045 GPS radio occultation. Geophysical Research Letters, 35(14), L14809. https://doi.org/10.1029/2008GL034158

KATAMZI-JOSEPH ET AL. 17 of 20

- Booker, J., & Bretherton, F. (1967). The critical layer for internal gravity waves in a shear flow. *Journal of Fluid Mechanics*, 27(3), 513–539. https://doi.org/10.1017/S0022112067000515
- Bowman, G. G., Fukao, S., Yamamoto, M., & Igarashi, K. (1994). MU-radar recorded field-aligned irregularities in the F2 region and associated sporadic-E disturbances. *Journal of Geomagnetism and Geoelectricity*, 46(10), 873–889. https://doi.org/10.5636/jgg.46.873
- Bristow, W. A., Greenwald, R. A., & Villian, J. P. (1996). On the seasonal dependence of medium-scale atmospheric gravity waves in the upper atmosphere at high latitudes. *Journal of Geophysical Research*, 101(A7), 15685–15699. https://doi.org/10.1029/96JA01010
- Burke, W. J., Martinis, C. R., Lai, P. C., Gentile, L. C., Sullivan, C., & Pfaff, R. F. (2016). C/NOFS observations of electromagnetic coupling between magnetically conjugate MSTID structures. *Journal of Geophysical Research: Space Physics*, 121(3), 2569–2582. https://doi. org/10.1002/2015JA021965
- Candido, C. M. N., Pimenta, A. A., Bittencourt, J. A., & Becker-Guedes, F. (2008). Statistical analysis of the occurrence of medium-scale traveling ionospheric disturbancesover Brazilian low latitudes using OI 630.0 nm emission all-sky images. *Geophysical Research Letters*, 35(17), L17105. https://doi.org/10.1029/2008GL035043
- Cosgrove, R. B., & Tsunoda, R. T. (2002). A direction-dependent instability of sporadic-E layers in the nighttime midlatitude ionosphere. Geophysical Research Letters, 29(18), 11-1-11-4. https://doi.org/10.1029/2002GL014669
- Cosgrove, R. B., & Tsunoda, R. T. (2004). Instability of the E-F coupled nighttime midlatitude ionosphere. *Journal of Geophysical Research*, 109(A4), A04305. https://doi.org/10.1029/2003JA010243
- Cowling, D. H., Webb, H. D., & Yeh, K. C. (1971). Group rays of internal gravity waves in a wind-stratified atmosphere. *Journal of Geophysical Research*, 76(1), 200–213. https://doi.org/10.1029/JA076i001p00213
- Ding, F., Wan, W., Xu, G., Yu, T., Yang, G., & Wang, J. (2011). Climatology of medium-scale traveling ionospheric disturbances observed by a GPS network in central China. *Journal of Geophysical Research*. *116*(A9), A09327. https://doi.org/10.1029/2011JA016545
- Duly, T. M., Chapagain, N. P., & Makela, J. J. (2013). Climatology of nighttime medium-scale traveling ionospheric disturbances (MSTIDs) in the Central Pacific and South American sectors. *Annals of Geophysics*, 31(12), 2229–2237. https://doi.org/10.5194/angeo-31-2229-2013
- Figueiredo, C. A. O. B., Takahashi, H., Wrasse, C. M., Otsuka, Y., Shiokawa, K., & Barros, D. (2018). Investigation of nighttime MSTIDS observed by optical thermosphere imagers at low latitudes: Morphology, propagation direction, and wind filtering. *Journal of Geophysical Research: Space Physics*, 123(9), 7843–7857. https://doi.org/10.1029/2018JA025438
- Fisher, D. J., Makela, J. J., Meriwether, J. W., Buriti, R. A., Benkhaldoun, Z., Kaab, M., & Lagheryeb, A. (2015). Climatologies of nighttime thermospheric winds and temperatures from Fabry-Perot interferometer measurements: From solar minimum to solar maximum. *Journal of Geophysical Research: Space Physics*, 120(8), 6679–6693. https://doi.org/10.1002/2015JA021170
- Fukushima, D., Shiokawa, K., Otsuka, Y., & Ogawa, T. (2012). Observations of equatorial nighttime medium-scale traveling ionospheric disturbances in 630-nm aiglow images over 7 years. *Journal of Geophysical Research*, 117(A10), A10324. https://doi.org/10.1029/2012JA017758
- Fuller-Rowell, T. J. (1998). The "thermospheric spoon": A mechanism for the semiannual density variation. *Journal of Geophysical Research*, 103(A3), 3951–3956. https://doi.org/10.1029/97JA03335
- Garcia, F. J., Kelley, M. C., Makela, J. J., & Huang, C. S. (2000). Airglow observations of mesoscale low-velocity traveling traveling ionospheric disturbances at midlatitudes. *Journal of Geophysical Research*, 105(A8), 18407–18415. https://doi.org/10.1029/1999JA000305
- Grocott, A., Hosokawa, K., Ishida, T., Lester, M., Milan, S. E., Freeman, M. P., et al. (2013). Characteristics of medium-scale traveling ionospheric disturbances observed near the Antarctic Peninsula by HF radar. *Journal of Geophysical Research: Space Physics*, 118(9), 1–12. https://doi.org/10.1002/jgra.50515
- Haldoupis, C., Pancheva, D., Singer, W., Meek, C., & MacDougall, J. (2007). An explanation for the seasonal dependence of midlatitude sporadic E layer. *Journal of Geophysical Research*, 112(A6), A06315, https://doi.org/10.1029/2007JA012322
- Hamza, A. M. (1999). Perkins instability revisited. Journal of Geophysical Research, 104(A10), 22567–22575. https://doi.org/10.1029/1999JA900307
- He, L.-S., Dyson, P. L., Parkinson, M. L., & Wan, W. (2004). Studies of medium scale travelling ionospheric disturbances using TIGER SuperD-ARN radar sea echo observations. Annals of Geophysics, 22(12), 4077–4088. https://doi.org/10.5194/angeo-22-4077-2004
- Hernandez-Pajares, M., Juan, J. M., & Sanz, J. (2006). Medium-scale traveling ionospheric disturbances affecting GPS measurements: Spatial and temporal analysis. *Journal of Geophysical Research*, 111(A7), A07S11. https://doi.org/10.1029/2005JA011474
- Hines, C. O. (1960). Internal atmospheric gravity waves at ionospheric heights. Canadian Journal of Physics, 38(11), 1441–1481. https://doi.org/10.1139/p60-150
- Hines, C. O., & Reddy, C. A. (1967). On the propagation of atmospheric gravity waves through regions of wind shear. *Journal of Geophysical Research*, 72(3), 1015–1034. https://doi.org/10.1029/JZ072i003p01015
- Huang, C. S., Miller, C. A., & Kelley, M. C. (1994). Basic properties and gravity wave initiation of the midlatitude F region instability. *Journal of Geophysical Research*, 29(1), 395–405. https://doi.org/10.1029/93RS01669
- Huang, F., Dou, X., Lei, J., Lin, J., Ding, F., & Zhong, J. (2016). Statistical analysis of nighttime medium-scale traveling ionospheric disturbances using airglow images and GPS observations over central China. *Journal of Geophysical Research*, 121(9), 8887–8899. https://doi.org/10.1002/2016JA022760
- Huang, F., Lei, J., Dou, X., Luan, X., & Zhong, J. (2018). Nighttime medium-scale traveling ionospheric disturbances from airglow imager and Global Navigation Satellite Systems observations. *Geophysical Research Letters*, 45(1), 31–38. https://doi.org/10.1002/2017GL076408
- Hunsucker, R. (1982). Atmospheric gravity waves generated in the high-latitude ionosphere: A review. Reviews of Geophysics, 20(2), 293–315. https://doi.org/10.1029/RG020i002p00293
- Jacobson, A. R., Robert, C. C., Massey, R. S., & Wu, G. (1995). Observations of traveling ionospheric disturbances with a satellite-beacon radio interferometer: Seasonal and local time behavior. *Journal of Geophysical Research*, 100(A2), 1653–1665. https://doi.org/10.1029/94JA02663
  Kelley, M. (2011). On the origin of mesoscale TIDs at midlatitudes. *Annales Geophysicae*, 29(2), 361–366. https://doi.org/10.5194/angeo-
- 29-361-2011

  Kelley, M. C., & Fukao, S. (1991). Turbulent upwelling of the mid-latitude ionosphere: 2. Theoretical framewrok. *Journal of Geophysical*
- Research, 96(A3), 3747–3753. https://doi.org/10.1029/90JA02252

  Kelley, M. C., Haldoupis, C., Nicolls, M. J., Makela, J. J., Belehaki, A., Shalimov, S., & Wong, V. K. (2003). Case studies of coupling between the E and F regions during unstable sporadic-E conditions. Journal of Geophysical Research, 108(A12), 1447. https://doi.org/10.1029/2003JA009955
- Kelley, M. C., & Makela, J. J. (2001). Resolution of the discrepancy between experiment and theory of midlatitude F-region structures. *Geophysical Research Letters*, 28(13), 2589–2592. https://doi.org/10.1029/2000GL012777
- Kelley, M. C., & Miller, C. A. (1997). Electrodynamics of midlatitude spread F3. Electrodynamic waves? A new look at the role of electric fields in thermospheric wave dynamics. *Journal of Geophysical Research*, 102(A6), 11539–11547. https://doi.org/10.1029/96JA03841
- Kil, H., & Paxton, L. (2017). Global distribution of nighttime meduim-scale traveling ionospheric disturbances seen by Swarm satellites. Geophysical Research Letters, 44(18), 9176–9182. https://doi.org/10.1002/2017GL074750

KATAMZI-JOSEPH ET AL. 18 of 20

- Kotake, N., Otsuka, Y., Ogawa, T., Tsugawa, T., & Saito, A. (2007). Statistical study of medium-scale traveling ionospheric disturbances observed with the GPS networks in Southern California. Earth Planets and Space, 59(2), 95–102. https://doi.org/10.1186/BF03352681
- Kotake, N., Otsuka, Y., Tsugawa, T., Ogawa, T., & Saito, A. (2006). Climatological study of GPS total electron content variations caused by medium-scale traveling ionospheric disturbances. *Journal of Geophysical Research*, 111(A4), A04306. https://doi.org/10.1029/2005JA011418
- Kubota, M., Conde, M., Ishii, M., Murayama, Y., & Jin, H. (2011). Characteristics of nighttime medium-scale traveling ionospheric disturbances observed over Alaska. *Journal of Geophysical Research*, 116(A5), A05307. https://doi.org/10.1029/2010JA016212
- Makela, J., Miller, E., & Talaat, E. (2010). Nighttime medium-scale traveling ionospheric disturbances at low geomagnetic latitudes. Geophysical Research Letters, 37(24), L24104. https://doi.org/10.1029/2010GL045922
- Martinis, C., Baumgardner, J., Mendillo, M., Wroten, J., McDonald, T., Kosch, M., et al. (2019). First conjugate observations of medium-scale traveling ionospheric disturbances (TIDs) in the Europe-Africa longitude sector. *Journal of Geophysical Research: Space Physics*, 124(3), 2213–2222. https://doi.org/10.1029/2018JA026018
- Martinis, C., Baumgardner, J., Wroten, J., & Mendillo, M. (2010). Seasonal dependence of MSTIDs obtained from 630.0 nm airglow imaging at Arecibo. Geophysical Research Letters, 37(11), L11103. https://doi.org/10.1029/2010GL043569
- Martinis, C., Baumgardner, J., Wroten, J., & Mendillo, M. (2011). All-sky imaging observations of conjugate medium-scale traveling ionospheric disturbances in the American sector. *Journal of Geophysical Research*, 116(A5), A05326. https://doi.org/10.1029/2010JA016264
- Martinis, C., Baumgardner, J., Wroten, J., & Mendillo, M. (2018). All-sky-imaging capabilities for ionospheric space weather research using geomagnetic conjugate point observing sites. Advances in Space Research, 61(7), 1636–1651. https://doi.org/10.1016/j.asr.2017.07.021
- Mayr, H., Harris, I., Varisi, R., & Herrero, R. (1984). Global excitation of wave phenomena in a dissipative multiconstituent medium: 1. Transfer
- function of the Earth's thermosphere. *Journal of Geophysical Research*, 89(A12), 10929–10959. https://doi.org/10.1029/JA089iA12p10929

  Mendillo, M., Baumgardner, J., Nottingham, D., Aarons, J., Reinisch, B., Scali, J., & Kelley, M. (1997). Investigations of thermosphere-ionospheric dynamics with 6300-Å images from the Arecibo Observatory. *Journal of Geophysical Research*, 102(A4), 7331–7343. https://doi.org/10.1029/96JA02786
- Miller, C. A., Swartz, W. E., Kelley, M. C., Mendillo, M., Nottingham, D., Scali, J., & Reinisch, B. (1997). Electrodynamics of midlatitude spread F1. Observations of unstable, gravity wave-induced ionospheric electric fields at tropical latitudes. *Journal of Geophysical Research*, 102(A6), 11521–11532. https://doi.org/10.1029/96JA03839
- Mondal, S., Srivastava, A., Yadav, V., Sarkhel, S., Krishna, M. S., Rao, Y. K., & Singh, V. (2019). Allsky airglow imaging observations from Hanle, Leh Ladakh, India: Image analyses and first results. Advances in Space Research, 64(10), 1926–1939. https://doi.org/10.1016/j. asr 2019 05 047
- Narayanan, V. L., Shiokawa, K., Otsuka, Y., & Neudegg, D. (2018). On the role of thermospheric winds and sporadic E layers in the formation and evolution of electrified MSTIDs in geomagnetic conjugate regions. *Journal of Geophysical Research: Space Physics*, 123(8), 6957–6980.
- Narayanan, V. L., Shiokawa, K., Otsuka, Y., & Saito, S. (2014). Airglow observations of nighttime medium-scale traveling ionospheric disturbances from Yonaguni: Statistical characteristics and low-latitude limit. *Journal of Geophysical Research: Space Physics*, 119(11), 9268–9282. https://doi.org/10.1002/2014JA020368
- Oinats, A. V., Kurkin, V., & Nishitani, N. (2015). Statistical study of medium-scale traveling ionospheric disturbances using SuperDARN Hokkaido ground backscatter data for 2011. Earth Planets and Space, 67(1), 22. https://doi.org/10.1186/s40623-015-0192-4
- Ojo, T. T., Katamzi-Joseph, Z. T., Chu, K. T., Grawe, M. A., & Makela, J. J. (2022). A climatology of the nighttime thermospheric winds over Sutherland, South Africa. Advances in Space Research, 69(1), 209–219. https://doi.org/10.1016/j.asr.2021.10.015
- Otsuka, Y., Onoma, F., Shiokawa, K., Ogawa, T., Yamamoto, M., & Fukao, S. (2007). Simultaneous observations of nighttime medium-scale traveling ionospheric disturbances and E region field-aligned irregularities at midlatitude. *Journal of Geophysical Research*, 112(A6), A06317. https://doi.org/10.1029/2005JA011548
- Otsuka, Y., Shiokawa, K., & Ogawa, T. (2004). Geomagnetically conjugate observations of medium-scale traveling ionospheric disturbances at midlatitude using all-sky airglow imagers. Geophysical Research Letters, 31(15), L15803. https://doi.org/10.1029/2004GL020262
- Otsuka, Y., Suzuki, K., Nakagawa, S., Nishioka, M., Shiokawa, K., & Tsugawa, T. (2013). GPS observations of medium-scale traveling ionospheric disturbances over Europe. Annals of Geophysics, 31(2), 163–172. https://doi.org/10.5194/angeo-31-163-2013
- Paznukhov, V., Altadill, D., Juan, J. M., & Blanch, E. (2020). Ionospheric tilt measurements: Application to traveling ionospheric disturbances climatology study. *Radio Science*, 55(2), e2019RS007012. https://doi.org/10.1029/2019RS007012
- Perkins, F. (1973). Spread F and ionospheric currents. *Journal of Geophysical Research*, 78(1), 218–226. https://doi.org/10.1029/JA078i001p00218

  Pimenta, A. A., Amorim, D. C. M., & Candido, C. M. N. (2008). Thermospheric dark bandstructures at low latitudes in the southern hemisphere under different solar activity conditions: A study using OI 630 nmemission all-sky images. *Geophysical Research Letters*, 35(16), L16103. https://doi.org/10.1029/2008GL034904
- Pimenta, A. A., Kelley, M. C., Sahai, Y., Bittencourt, J. A., & Fagundes, P. (2008). Thermospheric dark band structures observed in all-sky OI 630 nm emission images over the Brazilian low-latitude sector. *Journal of Geophysical Research*, 113(A1), A01307. https://doi. org/10.1029/2007JA012444
- Rajesh, P. K., Liu, J. Y., Lin, C. H., Chen, A. B., Hsu, R. R., Chen, C. H., & Huba, J. D. (2016). Space-based imaging of night-time medium-scale traveling ionospheric disturbances using FORMOSAT-2/ISUAL 630.0 nm airglow observations. *Journal of Geophysical Research: Space Physics*, 121(5), 4769–4781. https://doi.org/10.1002/2015JA022334
- Rathi, R., Yadav, V., Mondal, S., Sarkhel, S., Krishna, M. V. S., & Upadhayaya, A. K. (2021). Evidence for simultaneous occurrence of periodic and single dark band MSTIDs over geomagnetic low-mid latitude transition region. *Journal of Atmospheric and Solar-Terrestrial Physics*, 215, 105588. https://doi.org/10.1016/j.jastp.2021.105588
- Reinisch, B. W., & Galkin, I. A. (2011). Global ionospheric radio observatory (GIRO). Earth Planets and Space, 63(4), 377–381. https://doi.org/10.5047/eps.2011.03.001
- Saito, S., Yamamoto, M., Hashiguchi, H., Maegawa, A., & Saito, A. (2007). Observational evidence of coupling between quasi-periodic echoes and medium scale traveling ionospheric disturbances. *Annals of Geophysics*, 25(10), 2185–2194. https://doi.org/10.5194/angeo-25-2185-2007
- Sangalli, L., Partamies, N., Syrjäsuo, M., Enell, C.-F., Kauristie, K., & Mäkenen, S. (2011). Performance study of the new EMCCD-based all-sky cameras for auroral imaging. *International Journal of Remote Sensing*, 32(11), 2987–3003. https://doi.org/10.1080/01431161.2010.541505
- Shiokawa, K., Ihara, C., Otsuka, Y., & Ogawa, T. (2003). Statistical study of nighttime medium-scale traveling ionospheric disturbances using midlatitude airglow images. *Journal of Geophysical Research*, 108(A1), 1052. https://doi.org/10.1029/2002JA009491
- Shiokawa, K., Mori, M., Otsuka, Y., Oyama, S., & Nozawa, S. (2012). Motion of high-latitude nighttime medium-scale traveling ionospheric disturbances associated with auroral brightening. *Journal of Geophysical Research*, 117(A10), A10316. https://doi.org/10.1029/2012JA017928Shiokawa, K., Otsuka, Y., & Ogawa, T. (2006). Quasiperiodic southward moving waves in 630-nm airglow images in the equatorial thermosphere.
- Journal of Geophysical Research, 111(A6), A06301. https://doi.org/10.1029/2005JA011406

KATAMZI-JOSEPH ET AL. 19 of 20



# Journal of Geophysical Research: Space Physics

- 10.1029/2022JA030375
- Shiokawa, K., Otsuka, Y., & Ogawa, T. (2009). Propagation characteristics of nighttime mesospheric and thermospheric waves observed by optical mesosphere thermosphere imagers at middle and low latitudes. *Earth Planets and Space*, 61(4), 479–491. https://doi.org/10.1186/BF03353165
- Shiokawa, K., Otsuka, Y., Tsugawa, T., Ogawa, T., Saito, A., Ohshima, K., & Wilkinson, P. (2005). Geomagnetic conjugate observation of nighttime medium-scale and large-scale traveling ionospheric disturbances: FRONT3 campaign. *Journal of Geophysical Research*, 110(A5), A05303. https://doi.org/10.1029/2004JA010845
- Sivakandan, M., Martinis, C., Otsuka, Y., Chau, J. L., Norrell, J., Mielich, J., et al. (2022). On the role of E-F region coupling in the generation of nighttime MSTIDs during summer and equinox: Case studies over northern Germany. *Journal of Geophysical Research: Space Physics*, 127(5), e2021JA030159. https://doi.org/10.1029/2021JA030159
- Tsugawa, T., Kotake, N., Otsuka, Y., & Saito, A. (2007). Medium-scale traveling ionospheric disturbances observed by GPS receiver network in Japan: A short review. GPS Solutions, 11(2), 139–144. https://doi.org/10.1007/s10292-006-0045-5
- Tsugawa, T., Otsuka, Y., Coster, A. J., & Saito, A. (2007). Medium-scale traveling ionospheric disturbances detected with dense and wide TEC maps over North America. Geophysical Research Letters, 34(22), L22101. https://doi.org/10.1029/2007GL031663
- Tsunoda, R. T., & Cosgrove, R. B. (2001). Coupled electrodynamics in the nighttime midlatitude ionosphere. *Geophysical Research Letters*, 28(22), 4171–4174. https://doi.org/10.1029/2001GL013245
- Wu, D. L., Ao, C. O., Hajj, G. A., de la Torre Juarez, M., & Mannucci, A. J. (2005). Sporadic E morphology from GPS-CHAMP radio occultation. Journal of Geophysical Research, 110(A1), A01306. https://doi.org/10.1029/2004JA010701
- Yamamoto, M., Komoda, N., Fukao, S., Tsunoda, R. T., Ogawa, T., & Tsuda, T. (1994). Spatial structure of the E region field-aligned irregularities revealed by the MU radar. *Radio Science*, 29(1), 337–347. https://doi.org/10.1029/93RS01846
- Yeh, K. C., Webb, H. D., & Cowling, D. H. (1972). Evidence of directional filtering of travelling ionospheric disturbance. Nature; Physical Science, 235(59), 131–132. https://doi.org/10.1038/physci235131a0
- Yokoyama, T., Hysell, D. L., Otsuka, Y., & Yamamoto, M. (2009). Three-dimensional simulation of the coupled Perkins and Es-layer instabilities in the nighttime midlatitude ionosphere. *Journal of Geophysical Research*, 114(A3), A03308. https://doi.org/10.1029/2008JA013789
- Yokoyama, T., Yamamoto, M., Fukao, S., & Cosgrove, R. B. (2004). Three-dimensional simulation on generation of polarization electric field in the midlatitude E-region ionosphere. *Journal of Geophysical Research*, 109(A1), A01309. https://doi.org/10.1029/2003JA010238
- Zhou, Q., & Matthews, D. (2006). On the physical explanation of the Perkins instability. *Journal of Geophysical Research*, 111(A12), A12309. https://doi.org/10.1029/2006JA011696

KATAMZI-JOSEPH ET AL. 20 of 20